Tensile strength of unsaturated coarse and fine-grained soils

Bulolo, Sam; Leong, Eng Choon; Kizza, Richard

2021

Bulolo, S., Leong, E. C. & Kizza, R. (2021). Tensile strength of unsaturated coarse and fine-grained soils. Bulletin of Engineering Geology and the Environment, 80(3), 2727-2750. https://dx.doi.org/10.1007/s10064-020-02073-6

https://hdl.handle.net/10356/155895

https://doi.org/10.1007/s10064-020-02073-6

Bulolo, S., Leong, E.C. & Kizza, R. (2021). Tensile strength of unsaturated coarse and fine-grained soils. Bull Eng Geol Environ. https://doi.org/10.1007/s10064-020-02073-6

TENSILE STRENGTH OF UNSATURATED COARSE- AND FINE-GRAINED SOILS

S. Bulolo, E.C. Leong, and R. Kizza

ABSTRACT

Soils at the ground surface experience multiple cycles of drying and wetting. On drying, the soils experience shrinkage and cracks may appear. The development of cracks depends on the tensile strength of the soil. Such cracks increases the permeability of the soil and can cause slopes and earth structures to fail due to rainfall. Several tensile strength models have been proposed for unsaturated soils considering the effect of matric suction. However, the tensile strength models proposed are for either cohesionless (coarse-grained) or clayey (fine-grained) soils. The tensile strength models were shown to be different in their definition of suction stress and the presence or absence of a cohesion term. As tensile strength data of fine-grained soils with the same soil structure and soil-water characteristic curve data are lacking in the literature, Brazilian tensile tests and SWCC tests were conducted on compacted fine-grained soils from two residual soil formations. The test data highlighted the problem in the friction angle used in existing tensile strength models. Using a general form of the suction stress and the extended Mohr-Coulomb criterion with the Brazilian test Mohr circle, a new tensile strength model applicable to both coarse-grained and fine-grained soils was proposed. The proposed model was shown to perform better than existing models using independent data.

Keywords: Tensile strength; Brazilian test, matric suction; unsaturated soils

INTRODUCTION

Soils near the ground surface experience multiple drying and wetting cycles according to weather and climatic conditions. As soil dries, it experiences shrinkage and tensile cracks.

These cracks affect integrity of soil structures such as slopes, dams and embankments in terms of permeability and strength. Cracks in the soil provide an easy pathway for rainwater infiltration and such phenomenon is commonly associated with failures in slopes, dams and earth structures. Tensile cracks are highly influenced by the tensile strength of soils (Morris et al. 1992, Trabelsi et al. 2011, Vaniceek 2013, Shi et al. 2014, Li et al. 2019, Tang et al. 2019). Research shows that the tensile strength of unsaturated soils is mainly influenced by matric suction of the unsaturated soils (De Souza Villar et al. 2009, Yin and Vanapalli 2018).

Tensile strength tests for soils are generally grouped based on the method of load application: direct and indirect tensile tests. Direct tensile strength tests usually involve constraining one of the boundaries of the test specimen and applying uniaxial tensile force to the opposite boundary. The direct tensile test is regarded as the only method where a specimen is subjected to true uniaxial tension and failure occurs along its longitudinal axis (Peters and Leavell 1988, Win 2006). In a direct tensile test, it is assumed that uniform stresses are applied to the specimen, and torsional and bending stresses are absent. The tensile strength is computed as a ratio of the maximum load sustained by the specimen and the cross-sectional area upon which the load acts. Direct tensile strength tests have been conducted on soils (Tschebotarioff et al. 1953, Hasegawa and Ikeuti 1966, Ajaz and Parry 1975, Peters and Leavell 1988, Tang and Graham 2000, Trabelsi et al. 2010, Li et al. 2019, Murray and Tarantino 2019).

Despite the advantages of direct tensile strength test, the validity of the tests has been questioned due to difficulties associated with the test such as difficulty to effectively clamp or hold the specimen at the ends, misalignment, stress concentration and eccentric loading (Kennedy and Hudson 1968). Creep and volume changes as a result of sustained loading during the test have also been reported (Win 2006).

Bulolo, S., Leong, E.C. & Kizza, R. (2021). Tensile strength of unsaturated coarse and fine-grained soils. Bull Eng Geol Environ. https://doi.org/10.1007/s10064-020-02073-6

To address some of the difficulties in direct tensile tests, indirect tensile tests have been developed. Although the failure mode in indirect tensile test is a combination of compression and tension, indirect tensile tests have several advantages over direct tensile tests. It is relatively simple, failure is located in a region of uniform tensile strength, the specimens and equipment are the same as the compression tests, the surface conditions of the specimen does not affect the failure and less variation of the test results (Kennedy and Hudson 1968). Many studies have been conducted on soils using indirect tensile tests (e.g., Uchida and Matsumoto 1961, Kennedy and Hudson 1968, Khrishnayya and Eisenstein 1974, Dexter and Kroesbergen 1985, Das et al. 1995, Al-Hussaini 2009, Li and Wong 2013, Akin and Likos 2017, Pittaro 2019). Among the indirect tensile test, the Brazilian tensile strength (BTS) test is the most frequently used (Khrishnayya and Eisenstein 1974, Das et al. 1995, Vesga and Vallejo 2006, De Souza Villar et al. 2009, Beckett et al. 2015, Iravanian and Bilsel 2016, Akin and Likos 2017). Comparison between direct and indirect tensile tests show no significant differences between the tensile strength (e.g., Vesga and Vallejo 2006, Fahimifar and Malekpour 2012, Kim et al. 2012).

Several tensile strength models for unsaturated soils considering the effects of matric suction have been proposed. However, the tensile strength model is either for cohesionless (coarse-grained) soils or clayey (fine-grained) soils. Generally, tensile strength models considering the effects of matric suction have been developed for coarse-grained soils rather than for fine-grained soils and hence tensile strength data together with soil-water characteristic curve data for fine-grained soils are scarce in the literature. In some literature, unsaturated soils were prepared by compacting a soil at various water contents to the same dry density but the soils prepared in this manner have a different soil structure. Such data are not used in this study.

This study aims to develop a tensile strength model considering the effect of matric suction for both coarse and fine-grained soils. As tensile strength data for fine-grained soils with the same

soil structure and soil-water characteristic curve data are lacking in the literature, this study includes Brazilian tensile strength tests on fine-grained soils initially compacted wet of optimum and allowed to dry to various water contents. The matric suctions of the compacted soil specimens were measured using the contact filter paper method (ASTM D5298 − 16) as well as estimated from its soil-water characteristic curve (ASTM D6836-16).

TENSILE STRENGTH MODELS

Several theoretical models (Fisher 1926, Morris et al. 1992, Lu et al. 2009, Varsei et al. 2016) and empirical models (Kim and Hwang 2003, Munkholm and Kay 2014, Yin and Vanapalli 2018, Wang et al. 2020) have been developed to predict the tensile strength of soils. Tensile strength models based on the macromechanics approach compared to the micromechanical approach are more attractive for practical applications (Yin and Vanapalli, 2018). A summary of the tensile strength models based on the macromechanics approach is presented in Table 1. In Table 1, the models of Morris et al. (1992), Trabelsi et al. (2012), Tang et al. (2015), and Varsei et al. (2016) were developed for clayey soils while the models of Lu et al. (1992), Yin and Vanapalli (2018), and Wang et al. (2020) were developed for cohesionless soils. In most of the models shown in Table 1, the tensile strength σ_t of unsaturated soils is usually obtained from the Mohr-Coulomb criterion with the y-axis intercept given by the apparent cohesion c_{app} as shown in Figure 1. The σ_t is obtained from either direct uniaxial tensile test or indirect tensile test. If the uniaxial tensile test is used, the Mohr circle will have the minor principal stress as -σ_t and major principal stress as 0. Based on Figure 1, this case will give

$$\sigma_t = \frac{2\cos\phi_t}{1+\sin\phi_t} c^*_{app} \text{; or alternatively} \quad \sigma_t = 2\tan\left(\frac{\pi}{4}-\frac{\phi_t}{2}\right) c^*_{app} \tag{1}$$

The parameters of ϕ_t and c^*_{app} are defined in Figure 1.

If an indirect tensile test such as the Brazilian tensile test (ASTM D3967-16) is used, the Mohr circle will have the minor principal stress as $-\sigma_t$ and the major principal stress as about $3.1\sigma_t$ (Li and Wong 2013, Sivakugan et al. 2014, Consoli et al. 2015). In this case, σ_t is given by Equation 2.

$$\sigma_t = \frac{\cos\phi'}{\left(2.05 - 1.05\sin\phi'\right)} c_{app} \tag{2}$$

The parameters of ϕ' and c_{app} are defined in Figure 1.

Except for Snyder and Miller (1985) in Table 1, the other tensile strength models can be expressed in the form of either Equation 1 or 2 where c_{app} can be expressed in the form of the total cohesion in the extended Mohr-Coulumb criterion for unsaturated soils (Fredlund et al. 1978) as shown in Equation 3.

$$c_{app} = c' + \left(u_a - u_w\right)\tan\phi^b \tag{3}$$

where c' is the effective cohesion, u_a is pore-air pressure, u_w is pore water pressure and ϕ^b is the angle indicating the rate of shear strength increase due to matric suction (u_a-u_w). Equation 3 can also be expressed more generally in term of a suction stress σ^s as shown in Equation 4.

$$c_{app} = c' + \sigma^s \tan\phi' \tag{4}$$

In the tensile strength model of Morris et al. (1992), the coefficient of 0.5 based on Frydman (1967) and Baker (1981) and the coefficient of (0.5 to 0.7) cot ϕ' based on Bagge (1985) shown in Table 1 can be examined in the context of Equations 1 and 2. Figure 2 shows a plot of coefficient $\left(\frac{2\cos\phi_t}{1+\sin\phi_t}\right)$ from Equation 1 and coefficient $\left[\frac{\cos\phi'}{\left(2.05-1.05\sin\phi'\right)}\right]$ from Equation 2 versus the friction angle ϕ_t or ϕ' for the typical range from 15° to 50°. It can be seen that the

coefficient $\left(\frac{2\cos\phi_t}{1+\sin\phi_t}\right)$ is close to 0.7cot ϕ' for the range of ϕ' = ϕ_t from 28° to 40° and the coefficient $\left[\frac{\cos\phi'}{(2.05-1.05\sin\phi')}\right]$ is close to 0.5 for the full range of friction angle.

For the other tensile strength models in Table 1, Equation 1 is used and only differs in the definition of σ^s and the presence or absence of a cohesion term. The tensile strength models of Tang et al. (2015), Yin and Vanapalli (2018), and Wang et al. (2020) originated from Lu et al. (2009). The differences amongst these models lie in the definition of σ^s which can be expressed in the general form of Equation 5.

$$\sigma^s = S_e^k\left(u_a - u_w\right) + f \tag{5}$$

where S_e is the effective degree of saturation $\left(=\frac{S-S_r}{1-S_r}\right)$, S_r is the residual degree of saturation and exponent k is a parameter. The first term on the right-hand-side of Equation 5 is attributed to capillary suction while the second term (*f*) is attributed to surface tension of the "capillary bridges" (Yin and Vanapalli, 2018; Wang et al., 2020). Only the exponent k in Yin and Vanapalli (2018) model is not unity. Yin and Vanapalli (2018) relate k to be a function of van Genuchten (1980) soil-water characteristic curve (SWCC) equation parameter n and capillary degree of saturation S_c which is dependent on the coefficient of uniformity C_u. The equations are shown in Table 1. The effective degree of saturation S_e is defined differently in Varsei et al. (2016) who make use of a microscopic degree of saturation S_r^m following Alonso et al. (2010) instead of residual degree of saturation S_r as shown in Equation 6.

$$S_e^m = \frac{S-S_r^m}{1-S_r^m} = \left(S\right)^{\alpha^*} \tag{6}$$

Instead of determining S_r^m, Varsei et al. (2016) proposes Equation 7 where α* is a material parameter and is always equal to or greater than 1.

$$S_e^m = \left(S\right)^{\alpha^*} \tag{7}$$

The term *f* is zero in Lu et al. (2009), Trabelsi et al. (2012), Tang et al. (2015), and Varsei et al. (2016). Wang et al. (2020) followed Yin and Vanapalli (2018) formulation of *f* to be a product of surface tension of water T_s and the specific air-water interfacial area per pore volume a_{aw}, i.e. $f = T_s.a_{aw}$. The equations are given in Table 1.

Lu et al. (2009), Tang et al. (2015), Yin and Vanapalli (2018) and Wang et al. (2020) make use of the van Genuchten (1980) SWCC equation in their tensile strength model. However, Wang et al. (2020) propose equations to determine the van Genuchten (1980) SWCC equation parameters α and n, as shown in Table 1.

As the models of Lu et al. (1992), Yin and Vanapalli (2018), and Wang et al. (2020) were developed for cohesionless soils, the cohesion term is zero. However, three out of ten soils that Yin and Vanapalli (2018) used in the development of their model are fine-grained soils. In contrast, the models of Trabelsi et al. (2012), Tang et al. (2015), and Varsei et al. (2016) were developed for clayey soils and hence contain a cohesion term. Only Varsei et al. (2016) kept the cohesion term as the effective cohesion. In Trabelsi et al. (2012) model, the cohesion term is a function of porosity while in the Tang et al. (2012) model, the cohesion is given by the residual tensile strength at full saturation. However, Tang et al. (2015) model was developed for soils compacted at various water contents to the same dry density. Thus, Tang et al. (2015) model assume that the influence of the soil structure on σ_t, α, and n is negligible.

In summary, the macroscopic approach tensile strength models showed variations only in the definition of the suction stress σ^s and the presence of a cohesion term c for clayey soils only.

149 The general form of the macroscopic approach tensile strength model is expressed in Equation
150 8.

$$\sigma_t = 2\tan\left(\frac{\pi}{4}-\frac{\phi}{2}\right)\left(\sigma_s \tan\phi + c\right) \quad (8)$$

151 The suction stress σ^s consists of either one term (Lu et al. 2009, Tang et al. 2015, Varsei 2016)
152 or two terms (Yin and Vanapalli 2018, Wang et al. 2020).

153 In the development of the tensile strength model for unsaturated soils, the grain size distribution
154 curve, SWCC, and effective shear strength parameters for the saturated soil, c' and ϕ', are
155 required. The tensile strength tests should also be performed for a soil either undergoing drying
156 or wetting process and not on soils prepared at various water contents to avoid effects of soil
157 structure on the test results. Tensile strength test data with SWCC are more commonly found
158 for coarse-grained (cohesionless) soils than for fine-grained (clayey) soils in the literature,
159 hence tensile strength tests and SWCC tests are performed for fine-grained soils in this study.

160 **MATERIALS AND METHODS**

161 **Soil materials**

162 Two residual soils, one from the Bukit Timah Granite (BT) and the other from the Jurong
163 Formation (JF) in Singapore, were used as the fine-grained soils in this study**.** The Bukit Timah
164 Granite is mainly an acidic igneous rock system while the Jurong Formation is predominantly
165 a folded sedimentary rock system (Leong et al., 2002a). The basic properties of the two residual
166 soils are summarized in Table 2.

167 The standard (SP) and modified Proctor (MP) compaction curves of the residual soils according
168 to ASTM D698 - 12e2 and ASTM D1557-12e1 respectively are shown in Figure 3. The
169 maximum dry densities for the standard Proctor effort for BT and JF are 1.69 and 1.76 Mg/m^3,
170 respectively, corresponding to an optimum water content of 16% for both soils. The maximum

dry densities for the modified Proctor effort for BT and JF are 1.86 and 1.94 Mg/m^3, corresponding to optimum water contents of 13.3 and 13.5 %, respectively. The compaction properties of BT and JF residual soils are also included in Table 2. The preparation of the samples is described below.

Sample preparation and test procedures

Compaction

The air-dried residual soils were passed through sieve no. 4 and mixed with distilled water to the target moisture contents. The soils were then sealed in Ziploc bags and stored in a humidity chamber for at least five days to allow for moisture equalization.

To obtain test specimens of about 50 mm in diameter for the BTS test, a two-part split PVC cylindrical mold (internal diameter of 52 mm and height of 102 mm) was fabricated. A compaction apparatus was fabricated to ensure that the compaction procedure is consistent for the preparation of the soil samples. The compaction apparatus, shown in Figure 4, was equipped with a pulley system to lift a cylindrical drop mass of 4.5 kg and dimensions of 75 mm diameter and 150 mm height with a centre hole. The drop mass centre hole slides along a PVC tube guide which is slotted onto a dowel on top of a solid steel cylinder, diameter 51.6 mm and height of about 100 mm., which acts as the anvil. The anvil is placed on top of the soil in the PVC two-part split mold. A PVC collar sits on top of the PVC two-part split mold to constrain the anvil. The PVC two-part split mold is held together with hose clips and rests on the standard compaction mold base plate. The PVC two-part split mold is held upright at mid-height by an acrylic square plate with a center hole that is is held in place using the screws of the standard compaction mold base plate and nuts. The height of fall of the drop mass was calibrated to deliver standard and modified Proctor energies to the soil. For the standard Proctor energy, the drop mass falls through a height of 200 mm and the soil is compacted in three layers

while for the modified Proctor energy, the drop mass falls through a height of 450 mm and the soil is compacted in five layers. For both compaction energies, each layer in the PVC mold was subjected to six blows. The compacted sample produced has a height of about 100 mm.

Before each compaction, the internal walls of the PVC split mold were lightly oiled. During compaction, each layer was scarified before placing another layer to allow for bonding between the layers. The soils were compacted wet of optimum on both the standard and modified Proctor curves, indicated as A to D for BT soils and E to G for JF soils in Figures 3a and 3b, respectively. As each of these points are compacted at different water contents wet of optimum, the soil structure is different and thus each point can be said to be a “different” soil. For each point, A to G, multiple samples were prepared and collectively, these samples are denoted as sample sets A to G and the average soil properties are summarized in Table 3.

Brazilian tensile strength (BTS) test

Tensile strength of soil is commonly determined in the laboratory by direct and indirect tensile test methods. Although the indirect tensile test has been criticized as being less reliable, research has shown that the indirect tensile tests have advantages over the direct tensile test such as indirect tensile test is relatively simpler to perform; the specimens and equipment can be the same as for compression tests; the failure is located in a region of uniform tensile strength; the surface condition of the specimen does not affect the failure and there is less variability in the test results (Al-Hussaini and Townsend 1973, Vaniceek 2013, He et al. 2018).

The Brazilian tensile strength (BTS) test is an indirect tensile test originally developed for rock (ASTM D3967-16) but has been used to obtain the tensile strength of soils (e.g., Khrishnayya and Eisenstein 1974, Das et al. 1995, Vesga and Vallejo 2006, De Souza Villar et al. 2009, Beckett et al. 2015, Iravanian and Bilsel 2016, Akin and Likos 2017). A review on the development of the BTS test can be found in Li and Wong (2013). In the BTS test, the applied

load is compressive but the failure mode is tensile if specific constraints on specimen geometry (thickness to diameter, t/d, and ratio) are met. In ASTM D3967 – 16 the t/d ratio is recommended to be within the range of 0.2 to 0.75. Akin and Likos (2017) found that the tensile strength is essentially constant when t/d ratio is greater than 0.42 for kaolin. In this study, the t/d ratio of the test specimens was maintained as close to 0.6 as possible. Hence, each compacted sample of 100 mm length was sawn using Buehler IsoMet™ 4000 precision saw into three cylindrical disk specimens of about 30 mm thick and 52 mm diameter. Although the precision saw can minimize sample deformation and have low kerf loss, the compacted sample was wrapped in two layers of cling film followed by a single layer of masking tape along the sample height to prevent moisture loss and to limit surface cracking during sawing. The disk specimens were then dried to various water contents in airtight desiccators with saturated sodium chloride (NaCl) solution at the base of the desiccators. The saturated NaCl solution provides a constant relative humidity of about 76% (Young 1967) to dry the test specimens. Weight and volume of the disk specimens were measured regularly to provide the shrinkage curve. Test specimens that attained the targeted weight (and hence moisture content) were wrapped in cling film and thereafter kept in a temperature-controlled humidity chamber to allow for moisture equalization for about 10 days as recommended by Mendes (2011) before testing.

The test specimens for the BTS in this study were loaded using two specially fabricated curved bearing blocks as recommended in ASTM D3967 − 16 to reduce contact stress. The radius of the contact arc and width of contact with the test specimen were 10^{o} and 30 mm, respectively. During testing, the bearing blocks were attached to the loading platens of an unconfined compression test machine using magnets embedded into the base of the bearing block (Figure 5). The BTS test was conducted at a loading rate of 0.5 mm/min and all test specimens failed

243 within 1 to 10 minutes as recommended in ASTM D3967 − 16 The tensile strength σ_t was
244 computed from the BTS test results using Equation 9 (ASTM D3967 − 16).

245 $$\sigma_t = 1.272\frac{P}{\pi tD} \quad (9)$$

246 where P is the maximum applied load in the BTS test, t is the thickness of the specimen and D
247 is the diameter of the specimen. The number of tensile tests conducted for each sample set
248 ranges from 35 to 66 giving a total of 343 tensile test results. Observations during the BTS tests
249 show that crack initiated at the centre of the disk and the stress-displacement curves exhibited
250 brittle failure in almost all the tests indicating the general applicability of the BTS test for the
251 compacted soils in this study (Frdyman, 1964; 1967).

252 **Suction measurements**

253 Suction measurements were conducted on the compacted soil samples using the contact filter
254 paper method following Leong et al. (2002b). Whatman No. 42 filter paper of diameter 42.5
255 mm was used. The matric suction calibration equations for Whatman No. 42 filter paper used
256 were those suggested by Leong et al. (2002b) and reproduced in Equation 10.

$$\log \psi = \begin{cases} 2.909 - 0.0229 w_f, & w_f \geq 47 \\ 4.945 - 0.0673 w_f, & w_f < 47 \end{cases} \quad (10)$$

257 where ψ is the matric suction and w_f is the water content of the filter paper in %.

258 For the suction measurement, the compacted soil sample was sawn into four cylindrical disk
259 specimens of about 25 mm height each. A piece of filter paper was sandwiched between two
260 disk specimens and then wrapped in cling film and taped to minimize moisture loss as
261 suggested by Bulut et al. (2001). Each of the taped specimens was then placed in an airtight
262 container and kept in a constant temperature chamber for 28 days to allow for suction
263 equilibration. At the end of 28 days, procedures recommended by Bulut et al. (2001) were

followed to determine the water content w_f of the filter paper. The matric suction of the compacted soil was then computed using Equation 10.

Soil-water characteristic curves

The SWCCs of the compacted soils were established using both the pressure plate apparatus (method C) and the chilled-mirror dew-point technique (method D) following ASTM D6836-16. For suctions up to and including 1000 kPa, a pressure plate apparatus with a 15-bar ceramic plate cell was used. For suctions higher than 1000kPa, the WP4C dewpoint potentiometer (Leong et al. 2003) was used.

Before commencement of the pressure plate test, the compacted samples were saturated following the procedure suggested by Agus et al. (2001) and then to disk specimens of 50 mm diameter and 30 mm height were used. The suction level in the pressure plate extractor was increased incrementally from 10 to 1000 kPa as recommended in ASTM D6836-16. At equilibrium, the weight and volume of the specimens were measured to provide the shrinkage curve.

For the WP4C dewpoint potential meter, a cylindrical disk specimen of diameter 35 mm and thickness 5 mm was cookie-cut from the saturated compacted sample using a PVC ring with a sharpened edge and placed into the WP4C sample cups. These specimens in the sample cups were dried in airtight desiccators containing saturated NaCl solution. The weights of the sample cups with the soils were monitored periodically as the soil dries and concurrently, the suction was measured using the WP4C dewpoint potentiometer. The drying continued until no further change in weight could be observed (less than 0.001g). The sample cups with the soils were then left outside the desiccator (laboratory environment at 22 ± 4^{o}C and relative humidity at

~60%) to allow for further drying and measuring the suction using the WP4C dewpoint potentiometer until no further weight change could be detected (less than 0.001g).

RESULTS AND DISCUSSION

Tensile strength tests

The test results for sample sets A to D and E to F are summarized in Figures 6a and 6b, respectively. For all the sample sets, drying of the soil specimens from the wet of optimum to dry of optimum showed an increase in σ_t. The σ_t values increase up to a certain limit and then generally becomes constant despite further drying or increase in soil suction. Some data shows a slight drop in σ_t at extremely low water contents. The degree of saturation at which σ_t ceases to increase significantly varies between 95 and 97% for all the sample sets. Locating these degrees of saturation on the shrinkage curves indicate that they correspond approximately to the curvature of the shrinkage curve, which begins to depart from the 100% degree of saturation line and approaches the minimum void ratio. As the soil dries, its volume decreases and suction increases. These factors collectively influence σ_t. However, the contribution of suction to σ_t becomes increasingly minimal past the air-entry value (AEV) of the soil since the water phase becomes increasingly discontinuous in the soil. Hence, σ_t ceases to increase and becomes almost constant when the shrinkage limit is reached. Any deviation from the constant value is attributed to micro-fissures in the specimen and can be classified as experimental errors.

Evaluation of Tensile Strength Models

Review of the tensile strength models showed a general form and two variations of suction stress which can be represented by the models of Lu et al. (2009) and Yin and Vanapalli (2018). For evaluation of the tensile strength models, ϕ' is needed. The ϕ' values for sample sets A to G were obtained from consolidated undrained triaxial tests for saturated soil specimens of each sample set conducted following ASTM D4767-11 (details are reported in Kiiza, 2019). The

effective stress shear strength parameters (c' and ϕ') and the van Genuchten (1980) SWCC equation parameters (α and n) for sample sets A to G are tabulated in Table 4.

Lu et.al (2009) suggest that ϕ_t be obtained using a non-linear Mohr-Coulomb envelope in the low-stress zone and can be greater than the effective friction angle ϕ' (See Figure 1). For the presentation of results, two cases of ϕ_t values are shown, i.e.

Case 1: All parameters were as evaluated from experimental data, i.e. α and n of the van Genuchten (1980) SWCC equation from curve fitting the SWCC data while $\phi_t = \phi$' as given in Table 4.

Case 2: Values of α and n of the van Genuchten (1980) SWCC equation as for Case 1 while ϕ_t was adjusted to obtain the best match with the experimental data.

The performance of Lu et al. (2009) tensile strength model is shown in Figure 7. In Figure 7, the SWCC is also plotted. To evaluate the performance of the tensile strength model against the experimental data, the root mean square error (RMSE) was computed. The RMSE is defined in Equation 11.

$$RMSE = \sqrt{\frac{\sum_{i=1}^{n}\left(X_{obs,i} - X_{\mathrm{model},i}\right)^2}{n}} \tag{11}$$

where $X_{obs,i}$ = observed/measured value, $X_{model,i}$ = model value as predicted at the same conditions as observed value, n = number of data points. A smaller RMSE indicates a better agreement.

As expected, Case 2 gives the better estimate as compared to Case 1 for all sample sets A to G. The values of α and n of the van Genuchten (1980) SWCC equation seem too low for Lu et al.

(2009) tensile strength model to estimate the test data. In Case 2, the value of ϕ_t needs to be reduced from ϕ' to get a better match with the test data but there is no justification for the reduction in ϕ_t. Table 5 summarizes the ϕ_t and RMSE values for all the sample sets A to G. If a cohesion term was included in Lu et.al. (2009) tensile strength model, the value of ϕ_t would need to be further reduced to achieve a good match with the test data.

Similar to Lu et.al (2009) tensile strength model, Yin and Vanapalli (2018) tensile strength model could not estimate the test data well. For the presentation of results, two cases that gave the best estimate of the test data are presented:

Case 1: The parameters k and η_s were computed using the equations in Table 1while $\phi_t = \phi'$.

Case 2: The parameters k and η_s, were as for Case 1, while ϕ_t was adjusted to give the best match with the experimental data.

The void ratio e in Equation 8 is taken to be e_{min} from the shrinkage curve (Leong and Wijaya (2015). For the computation of k, the ratio S_0/S_c was set at 0.9 and 0.6 for BT and JF soils, respectively, within the range of values given by Yin and Vanapalli (2018).

Figure 8 shows the two cases where σ_t is plotted against S for all the sample sets A to G together with their SWCCs. Table 6 summarizes the parameters and the RMSE values for all the sample sets A to G. As expected, Case 2 gives the lower RMSE for all the sample sets. Similar to Lu et.al (2009) tensile strength model, ϕ_t in Yin and Vanapalli (2018) model needs to be reduced from ϕ' to obtain a better match with the test data and a further reduction is needed if a cohesion term is included in Yin and Vanapalli (2018) model. The model requires the use of either larger values of k and η_s or a smaller ϕ_t value to get a better match.

In both Lu et al. (2009) and Yin and Vanapalli (2018) tensile strength models, a better estimate of σ_t can only be obtained by using $\phi_t < \phi'$ as shown in Tables 5 and 6. This is undesirable as

ϕ_t becomes a fitting parameter and the model cannot be used in the predictive sense. Hence a more suitable tensile strength model needs to be developed keeping $\phi_t = \phi'$ to get a better estimate of σ_t.

PROPOSED TENSILE STRENGTH MODEL

Development

As mentioned earlier, Equation 1 is generic to the tensile strength models of Lu et al. (2009), Trabelsi et al. (2012), Yin and Vanapalli (2018), Tang et al. (2015), Varsei et al. (2016) and Wang et al. (2020). However, the friction angle is not ϕ' for the models of Lu et al. (2009), Tang et al. (2015) and Yin and Vanapalli (2018). By assuming that the extended Mohr-Coulomb criterion is tangent to the BTS test Mohr circle, Equation 2 was adopted instead. The biggest difference in the tensile strength models lies in the definition of σ^s. The σ^s can be made more general by adopting the form given in Equation 12.

$$\sigma^s = A.S^{k_1}.\left(u_a - u_w\right) \tag{12}$$

In Equation 12, A is a constant and is function of basic soil properties; degree of saturation S is used which implies that $S_r = 0$; exponent k_1 is used instead of k to indicate that it is a different exponent from that used in Yin and Vanapalli (2018). Similar non-linear suction stress-matric suction relationship as given in Equation 12 has been suggested by others, e.g. Kim et al. (2010). The proposed model is thus given by Equation 13.

$$\sigma_t = \frac{\cos\phi'}{\left(2.05 - 1.05\sin\phi'\right)}\left[\sigma^s \tan\phi' + c'\right] \tag{13}$$

According to Yin and Vanapalli, the exponent k is heavily related to the SWCC through van Genuchten (1980) SWCC equation parameter n and the capillary degree of saturation

corresponding to the AEV (S_c) and somewhat related to the grain size gradation parameter C_u. Hence, it is reasonable to suggest that k_1 is a function of parameters associated with void ratio e, grain size distribution and SWCC. It is highly likely that both A and k_1 have different expressions for coarse and fine-grained soils. Hence, expressions for A and k_1 were obtained separately for coarse and fine-grained soils. The soil properties used to obtain the proposed model parameters are α and n of VG SWCC equation (S_r = 0), void ratio e, gradation parameters, d_{50}, C_u and C_c, and percentage passing no. 200 sieve, P_{200}. A summary of the soil parameters used is tabulated in Table 7. For the coarse-grained soils, Ottawa sand from Goulding (2006), Perth sand, Silty and Fine sand from Lu et al. (2007) and Medium and Esperance sand from Lu et al. (2009) were used to develop the relationships for the proposed model parameters, A and k_1. For the fine-grained soils, the data reported in this study together with the mine tailings from Narvaez et al. (2015) were used to develop the relationships for the proposed model parameters, A and k_1.

To determine the relationships of parameters, A and k_1, with basic soil properties, an iterative optimization process was adopted. In the first iteration, the best-fit values of A and k_1 to each dataset in the calibration dataset were determined. A correlation matrix between A and k_1 with the basic soil properties and combinations (α, n, e, d_{50}, C_c, C_u, P_{200}, $\alpha.C_u$, $\alpha.C_c$, $n.C_u$, $n.C_c$, $e.P_{200}$, e.n) was determined. A regression analysis (using common functions of linear, exponential, power and quadratic polynomial) was then performed on the parameter (A or k_1) with the basic soil property or combination having the highest value in the correlation matrix. When more than one basic soil property or combination have the highest correlation values within 0.01, regression analysis was performed on each soil property or combination and the regression equation with the highest coefficient of determination R^2 was selected. Once the regression equation was obtained for the parameter (A or k_1), the value of the parameter was given by the regression equation while the other parameter (k_1 or A) were optimized again for

each dataset of the calibration dataset. Subsequently, a regression analysis (using common functions of linear, exponential, power and quadratic polynomial) was then performed on the other parameter. Finally, the coefficients of the regression equations obtained for parameters A and k_1 are optimized with the calibration dataset to obtain the final regression equations.

The correlation matrices for the coarse-grained and fine-grained soils are shown in Tables 8 and 9, respectively. For coarse-grained soils, parameter A has the highest correlation with C_c (0.9247) while parameter k_1 has the highest correlation with $n.C_c$ (-0.7230). As the correlation between parameter A and C_c is higher than the correlation between k_1 and $n.C_c$, a regression analysis was performed for parameter A with C_c as the independent variable to give Equation 14.

$$A = 9.973\left(C_c\right)^{6.2} \qquad \left(R^2 = 0.9010\right) \tag{14}$$

Using Equation 14 to give the value of parameter A for each dataset in the calibration dataset, values of k_1 were then optimized again to give k_{1_2} and a new correlation matrix is formed for k_{1_2} as shown in the last row of Table 8. The values of k_{1_2} have the highest correlation with $n.C_c$ (-0.7890). This correlation value is higher than the previous correlation between k_1 and $n.C_c$ (-0.7230). Hence, a regression equation was obtained for k_{1_2} with $n.C_c$ as the independent variable to give Equation 15.

$$k_{1\_2} = 2.835\exp\left(-0.341\cdot n\cdot C_c\right) \qquad \left(R^2 = 0.7031\right) \tag{15}$$

Finally, the coefficients of the regression equations for parameters A and k_{1_2} (Equations 14 and 15, respectively) were optimised with the calibration dataset to give the final equations, Equations 16 and 17, respectively. Note the slight changes in coefficients between Equations 14 and 16 for parameter A, and between Equations 15 and 17 for parameter k_1.

$$A = 9.869\left(C_c\right)^{6.405} \tag{16}$$

$$k_1 = 2.643\exp\left(-0.326 \cdot n \cdot Cc\right) \quad (17)$$

420

421 For fine-grained soils, parameter A has the highest correlations with C_c (0.9859) and $n.C_c$
422 (0.9815) while parameter k_1 has the highest correlation with e.n (-0.9289) (Table 9). As the
423 correlations between parameter A and C_c and between parameter A and $n.C_c$ are higher than
424 between k_1 and e.n, a regression analysis was performed for parameter A with C_c and $n.C_c$ as
425 an independent variable in turn. The regression equation for parameter A adopted was the one
426 with the highest coefficient of determination, R^2, shown in Equation 18.

$$A = 0.0255\left(C_c\right)^2 + 0.971Cc + 0.249 \qquad \left(R^2 = 0.9722\right) \quad (18)$$

427 Using Equation 18 to give the value of parameter A for each dataset of the calibration dataset,
428 the values of k_1 are then optimized for the calibration dataset again to give k_{1_2} and a new
429 correlation matrix is formed for k_{1_2} as shown in the last row of Table 9. The values of k_{1_2}
430 have the highest correlation with n (-0.9198) and e.n (-0.9294). Hence, a regression equation
431 was obtained for k_{1_2} with n and e.n as the independent variable in turn. The regression equation
432 for k_{1_2} adopted was the one with the highest coefficient of determination, R^2, shown in
433 Equation 19.

$$k_{1\_2} = 11.293\exp\left(-1.121n\right) \qquad \left(R^2 = 0.9279\right) \quad (19)$$

434

435 Finally, the coefficients of the regression equations for parameters A and k_{1_2} (Equations 18
436 and 19, respectively) were optimised with the calibration dataset to give the final equations,
437 Equations 20 and 21, respectively. Note the slight changes in coefficients between Equations
438 18 and 20 for parameter A, and between Equations 19 and 21 for parameter k_1.

$$A = -0.395\left(C_c\right)^2 + 1.784Cc + 0.041 \quad (20)$$

$$k_1 = 14.115\exp\left(-1.241n\right) \quad (21)$$

439

440 **Validation**

441 For validation of the proposed tensile strength model, three coarse-grained soils from Win
442 (2006), Kim and Sture (2008) and Jindal et al. (2016) and three fine-grained soils from Zeh
443 and Witt (2005), Wong et al. (2017) and Murray and Tarantino (2019) were used. These data
444 were not used in the derivation of the proposed tensile strength model. Most important of all,
445 these data are for soils of the same soil structure and contain the SWCC information. The
446 parameters of the validation dataset used in the proposed model are summarized in Table 10.
447 The performances of the modified tensile strength model, Lu et al. (2009) and Yin and
448 Vanapalli (2018) models are shown in Figures 9 and 10 for coarse and fine-grained soils,
449 respectively. The proposed model showed good agreement for the coarse and the fine-grained
450 soils in Figures 9 and 10 except for Figure 10a at high degree of saturation (> 80%). The data
451 in Figure 10a was for a medium plasticity clay which shrinks on drying (Zeh and Witts, 2005).
452 For such a soil it is expected that the soil remains fully saturated as the soil shrinks on drying
453 and only becomes less than fully saturated near the air-entry value. Hence, the data at high
454 degree of saturation were affected by error in the volume measurement. The RMSE for each
455 set of data are shown in Table 11. Figures 9 and 10, and Table 11 show that the proposed tensile
456 strength model outperforms Lu et al. (2009) and Yin and Vanapalli (2018) tensile strength
457 models.

458 **CONCLUSION**

459 This study reviews the macroscopic approach tensile strength models proposed for unsaturated
460 soils. The tensile strength models were proposed for either cohesionless (coarse-grained) or

clayey (fine-grained) soils. The differences and discrepancies of the models were highlighted. Brazilian tensile tests were performed on fine-grained soils compacted on the wet side of optimum and subjected to drying at various water contents. Existing tensile strength models for unsaturated soils were not able to model the tensile strength for a wide range of soil types. Using the test data together with data collated from the literature, a new tensile strength model was developed for both unsaturated coarse-grained and fine-grained soils. The proposed model uses the Brazilian tensile test Mohr Circle and the extended Mohr-Coulomb criterion. Parameters of the suction stress in the proposed model were related to the grain size distribution and soil-water characteristic curve. Using a validation data set of three coarse-grained soils and three fine-grained soils, the proposed tensile strength model was shown to perform better than existing tensile strength models.

ACKNOWLEDGEMENT

The first and third authors acknowledge the Singapore International Graduate Award (SINGA) scholarship for this PhD study.

DECLARATION

Funding

Not applicable

Conflicts of interest/Competing interests

None

Availability of data and material

Available upon reasonable request

Code availability (software application or custom code)

Not applicable

Bulolo, S., Leong, E.C. & Kizza, R. (2021). Tensile strength of unsaturated coarse and fine-grained soils. Bull Eng Geol Environ. https://doi.org/10.1007/s10064-020-02073-6

Authors' contributions

The second author (EC Leong) contributed to the study conception and design. Data collection and analysis were performed by the first author (Sam Bulolo). The manuscript was prepared by Sam Bulolo and EC Leong. The third author (Richard Kizza) provided the test data for the fine-grained soils reported in the manuscript.

REFERENCES

Agus, S.S., Leong, E.C., and Rahardjo, H. 2001. Soil-water characteristic curves of Singapore residual soils. Geotechnical and Geological Engineering, **19**(3–4): 285–309. doi:10.1023/A:1013175913679.

Ajaz, A., and Parry, R.H.G. 1975. Stress-Strain Behaviour of Two Compacted Clays in Tension and Compression. Geotechnique, 25(3): 495–512. doi:10.1680/geot.1975.25.3.495.

Akin, I.D., and Likos, W.J. 2017. Brazilian tensile strength testing of compacted clay. Geotechnical Testing Journal, **40**(4): 608–617. doi:10.1520/GTJ20160180.

Al-Hussaini, M.M., and Townsend, F.C. 1973. Tensile Testing of Soils: A Literature Review. *In* Misc Paper S73-24. USAE Waterways Research Station, Vicksburg, Missisippi. pp. 36–68.

Alonso, E.E., Pereira, J.-M., Vaunat, J., and Olivella, S. 2010. A microstructurally based effective stress for unsaturated soils. Géotechnique, **60**(12): 913–925. doi:10.1680/geot.8.P.002.

ASTM D1557-12e1. 2015. Standard test methods for laboratory compaction characteristics of soil using Modified Effort. West Conshohocken, PA. doi:10.1520/D1557-12.1, www.astm.org.

ASTM D3967 − 16. 2008. Standard Test Method for Splitting Tensile Strength of Intact Rock Core Specimens. West Conshohocken, PA. doi:10.1520/D3967-08.2.

ASTM D4767 -11. 2011. Standard Test Method for Consolidated Undrained Triaxial Compression Test for Cohesive Soils. West Conshohocken, PA. doi:10.1520/D4767-11.2.

ASTM D5298 − 16. 2016. Standard Test Method for Measurement of Soil Potential(Suction) Using Filter Paper. ASTM International, West Conshocken, PA, 2016,: 1–6. doi:10.1520/D5298-16.2.

ASTM D6836-16. 2016. Standard Test Methods for Determination of the Soil Water Chararcteristic Curve for Desorption Using a Hanging Column , Pressure Extractor , Chilled Mirror Hygrometer , or Centrifuge. West Conshohocken, PA.

ASTM D698 - 12e2. 2015. Standard test methods for laboratory compaction characteristics of soil using standard effort. West Conshohocken, PA. doi:DOI: 10.1520/D0698-12E01, www.astm.org.Bagge, G. 1985. Tension cracks in saturated clay cuttings. Proceedings of 11th International Conference on Soil Mechanics and Foundations Engineering, San Francisco, vol. 2, pp. 393-395.

Baker, R. 1981. Tensile strength, tension cracks, and stability of slopes. Soils and Foundations, **21**(2): 1–17.

Beckett, C.T.S., Smith, J.C., Ciancio, D., and Augarde, C.E. 2015. Tensile strengths of flocculated compacted unsaturated soils. Geotechnique Letters, 5(4): 254–260. doi:10.1680/jgele.15.00087.

Bulut, R., Lytton, R.L., and Wray, W.K. 2001. Soil Suction Measurements by Filter Paper. *In*

Bulolo, S., Leong, E.C. & Kizza, R. (2021). Tensile strength of unsaturated coarse and fine-grained soils. Bull Eng Geol Environ. https://doi.org/10.1007/s10064-020-02073-6

Proceedings of Expansive Clay Soils and Vegetative Influence on Shallow Foundations-. pp. 243–261.

Consoli, N.C., Festugato, L., Consoli, B.S., and Lopes, L.S. 2015. Assessing failure envelopes of soil-fly ash-lime blends. Journal of Materials in Civil Engineering, **27**(5): 1–9. doi:10.1061/(ASCE)MT.1943-5533.0001134.

Cuisinier, O., and Laloui, L. 2004. Fabric evolution during hydromechanical loading of a compacted silt. International Journal for Numerical and Analytical Methods in Geomechanics, **28**(6): 483–499. doi:10.1002/nag.348.

Das, B.M., Yen, S., and Dass, R. 1995. Brazilian tensile strength test of lightly cemented sand. Canadian Geotechnical Journal, 32(1): 166–171. doi:10.1139/t95-013.

De Souza Villar, L.F., De Campos, T.M.P., Azevedo, R.F., and Zornberg, J.G. 2009. Tensile strength changes under drying and its correlations with total and matric suctions. *In* Proceedings of the 17th International Conference on Soil Mechanics and Geotechnical Engineering: The Academia and Practice of Geotechnical Engineering. Alexandria, Egypt. pp. 793–796. doi:10.3233/978-1-60750-031-5-793.

Dexter, A.R., and Kroesbergen, B. 1985. Methodology for determination of tensile strength of soil aggregates. Journal of Agricultural Engineering Research, 31(2): 139–147. doi:10.1016/0021-8634(85)90066-6.

Fahimifar, A., and Malekpour, M. 2012. Experimental and numerical analysis of indirect and direct tensile strength using fracture mechanics concepts. Bulletin of Engineering Geology and the Environment, **71**(2): 269–283. doi:10.1007/s10064-011-0402-7.

Fisher, R.A. 1926. On the capillary forces in an ideal soil; correction of formulae given by W. B. Haines. The Journal of Agricultural Science, **16**(3): 492–505. doi:10.1017/S0021859600007838.

Fredlund, D.G., Morgenstern, N.R., and Widger, R.A. 1978. The shear strength of unsaturated soils. Canadian Geotechnical Journal, 15: 313-321.

Frydman, S., 1964, Applicability of the Brazilian (indirect tension) test to soils. Australian Journal Applied Science, 15(4): 335–343.

Frydman, S. 1967. Triaxial and tensile strength tests on stabilized soil. *In* 3rd Asian Regional Conference on Soil Mechanics and Foundations Engineering. Haifa. pp. 269–275.

Goulding, R.B. 2006. Tensile strength, shear strength, and effective stress for unsaturated sand. University of Missouri, Columbia. doi:10.19744/j.cnki.11-1235/f.2006.09.027.

Hasegawa, H., and Ikeuti, M. 1966. On the Tensile Strength Test of Disturbed Soils. *In* Rheology and Soil Mechanics / Rhéologie et Mécanique des Sols. *Edited by* P. Kravtdrenco, J. and Sirieys and M. Springer, Berlin, Heidelberg. pp. 405–412. doi:10.1007/978-3-662-39449-6_33.

He, S., Bai, H., and Xu, Z. 2018. Evaluation on tensile behavior characteristics of undisturbed loess. Energies, **11**(8): 1–18. doi:10.3390/en11081974.

Heibrock, G., Zeh, R.M., and Witt, K.J. 2005. Tensile Strength of Compacted Clays. *In* Unsaturated Soils: Experimental Studies. Berlin, Heidelberg. pp. 395–412. doi:10.1007/3-540-26736-0_30.

Iravanian, A., and Bilsel, H. 2016. Tensile Strength Properties of Sand-bentonite Mixtures Enhanced with Cement. Procedia Engineering, **143**(Ictg): 111–118. Elsevier B.V. doi:10.1016/j.proeng.2016.06.015.

Kennedy, T.W., and Hudson, W.R. 1968. Application of the Indirect Tensile Test To Stabilized Materials. Highway Research Board. Available from http://onlinepubs.trb.org/Onlinepubs/hrr/1968/235/235-004.pdf.

Khrishnayya, A.V., and Eisenstein, Z. 1975. Brazilian Tensile Test for Soils. Canadian Geotechnical Journal, **11**(4): 632–642. doi:DOI: 10.1139/t74-064.

Kiiza, R. 2019. Suction, hydraulic and strength properties of compacted soils. Nanyang

Bulolo, S., Leong, E.C. & Kizza, R. (2021). Tensile strength of unsaturated coarse and fine-grained soils. Bull Eng Geol Environ. https://doi.org/10.1007/s10064-020-02073-6

Technological University, Singapore.

Kim, B.., Shibuya, S., Park, S.., and Kato, S. 2010. Application of suction stress for estimating unsaturated shear strength of soils using direct shear testing under low confining pressure. Canadian Geotechnical Journal, **47**(9): 955–970.

Kim, T.H., and Hwang, C. 2003. Modeling of tensile strength on moist granular earth material at low water content. Engineering Geology, **69**(3–4): 233–244. doi:10.1016/S0013-7952(02)00284-3.

Kim, T.H., and Sture, S. 2008. Capillary-induced tensile strength in unsaturated sands. Canadian Geotechnical Journal, **45**(5): 726–737. doi:10.1139/T08-017.

Koliji, A., Laloui, L., Cusinier, O., and Vulliet, L. 2006. Suction induced effects on the fabric of a structured soil. Transport in Porous Media, **64**(2): 261–278. doi:10.1007/s11242-005-3656-3.

Leong, E.., He, L., and Rahardjo, H. 2002a. Factors Affecting the Filter Paper Method for Total and Matric Suction Measurements. Geotechnical Testing Journal, **25**(3): 1–12. doi:10.1520/GTJ11094J.

Leong, E.., Tripathy, S., and Rahardjo, H. 2003. Total suction measurement of unsaturated soils with a device using the chilled-mirror dew-point technique. Géotechnique, **53**(2): 173–182.

Leong, E.C., and Wijaya, M. 2015. Universal soil shrinkage curve equation. Geoderma, **237**: 78–87. Elsevier B.V. doi:10.1016/j.geoderma.2014.08.012.

Leong, E.C., Rahardjo, H., and Tang, S.K. 2002b. Characterisation and engineering properties of Singapore residual soils. *In* Proceedings of the International Workshop on Characterisation and Engineering Properties of Natural Soils, Singapore, 2. pp. 1279-1304.

Li, H.D, Tang, C.S., Cheng, Q., Li, S.J., Gong, X.P., and Shi, B. 2019. Tensile strength of clayey soil and the strain analysis based on image processing techniques. Engineering Geology, **253**(March): 137–148. Elsevier. doi:10.1016/j.enggeo.2019.03.017.

Li, D., and Wong, L.N.Y. 2013. The Brazilian disc test for rock mechanics applications: review and new insights. Rock mechanics and rock engineering **46** (2), 269-287.

Lu, N., Kim, T.-H., Sture, S., and Likos, W.J. 2009. Tensile Strength of Unsaturated Sand. Journal of Engineering Mechanics, **135**(12): 1410–1419. doi:10.1061/(ASCE)EM.1943-7889.0000054.

Lu, N., Wu, B., and Tan, C.P. 2007. Tensile Strength Characteristics of Unsaturated Sands. Journal of Geotechnical and Geoenvironmental Engineering, **133**(2): 144–154. doi:10.1061/(ASCE)1090-0241(2007)133:2(144).

Mendes, J. 2011. Assessment of the impact of climate change on an instrumented embankment: An unsaturated soil mechanics approach, Durham theses. Durham University. Available from online: http://etheses.dur.ac.uk/612/.

Morris, P.H., Graham, J., and Williams, D.J. 1992. Cracking in drying soils. Canadian Geotechnical Journal, **29**(2): 263–277. doi:10.1139/t92-030.

Munkholm, L.J., and Kay, B.D. 2014. Effect of Water Regime on Aggregate-tensile Strength, Rupture Energy, and Friability. Soil Science Society of America Journal, **66**(3): 702. doi:10.2136/sssaj2002.7020.

Murray, I., and Tarantino, A. 2019. Mechanisms of failure in saturated and unsaturated clayey geomaterials subjected to (total) tensile stress. Geotechnique, **69**(8): 701–712. doi:10.1680/jgeot.17.P.252.

Narvaez, B., Aubertin, M., and Saleh-Mbemba, F. 2015. Determination of the tensile strength of unsaturated tailings using bending tests. Canadian Geotechnical Journal, **52**(11): 1874–1885. doi:10.1139/cgj-2014-0156.

Peters, J., and Leavell, D. 1988. Relationship Between Tensile and Compressive Strengths of

Bulolo, S., Leong, E.C. & Kizza, R. (2021). Tensile strength of unsaturated coarse and fine-grained soils. Bull Eng Geol Environ. https://doi.org/10.1007/s10064-020-02073-6

Compacted Soils. *In* Advanced Triaxial Testing of Soil and Rock, ASTM STP 9. *Edited by* R.T. Donaghe, R.C. Chancy, and M.L. Silver. American Society for Testing and Materials, Philadelphia. pp. 169–188. doi:10.1520/stp29077s.

Pittaro, G. 2019. Tensile strength behaviour of Ground Improvement and its importance on deep excavations using deep soil. *In* XVII European conference on soil mechanics and geotechnical engineering. pp. 1–8. doi:10.32075/17ECSMGE-2019-0085.

Shi, B., Chen, S., Han, H., and Zheng, C. 2014. Expansive Soil Crack Depth under Cumulative Damage. The scientific world journal, **2014**: 1–9. doi:http://dx.doi.org/10.1155/2014/498437 Research.

Sivakugan, N., Das, B.M., Lovisa, J., and Patra, C.R. 2014. Determination of c and Φ of rocks from indirect tensile strength and uniaxial compression tests. International Journal of Geotechnical Engineering, **8**(1): 59–65. doi:10.1179/1938636213Z.00000000053.

Sun, W.J., and Cui, Y.J. 2017. Investigating the microstructure changes for silty soil during drying. Geotechnique, **68**(4): 370–373. doi:10.1680/jgeot.16.P.165.

Snyder, V.A., and Miller, R.D. 1985. Tensile strength of unsaturated soils. Soil Science Society of America Journal, 49(1): 58–65. doi:10.2136/sssaj1985.03615995004900010011x.

Tang, C.S., Pei, X.J., Wang, D.Y., Shi, B., and Li, J. 2015. Tensile Strength of Compacted Clayey Soil. Journal of Geotechnical and Geoenvironmental Engineering, **141**(4): 04014122_ 1–8. doi:10.1061/(ASCE)GT.1943-5606.0001267.

Tang, G.X., and Graham, J. 2000. A Method for Testing Tensile Strength in Unsaturated Soils. Geotechnical Testing Journal, **23**(3): 377–382. doi:10.1520/gtj11059j.

Tang, L., Zhao, Z., Luo, Z., and Sun, Y. 2019. What is the role of tensile cracks in cohesive slopes? Journal of Rock Mechanics and Geotechnical Engineering, **11**(2): 314–324. Elsevier Ltd. doi:10.1016/j.jrmge.2018.09.007.

Tarantino, A. 2010. Unsaturated soils: compacted versus reconstituted states. *In* 5th International Conference on Unsaturated Soil , Barcelona, Spain. pp. 113-136. doi:https://doi.org/10.1201/b10526-9.

Trabelsi, H., Jamei, M., Zenzri, H., and Olivella, S. 2012. Crack patterns in clayey soils: experiments and modeling. International Journal for Numerical and Analytical methods in Geomechanics, 36(11): 1410–1433. doi:10.1002/nag.1060.

Tschebotarioff, G., Ward, E., and Dephippe, A. 1953. The Tensile Strength of Disturbed and Recompacted Soils. *In* 3rd International Conference on Soil Mechanics and Foundation Engineering. Switzerland. pp. 207–210.

Uchida, I., and Matsumoto, R. 1961. On the test of the modulus of rupture of soil sample. Soils and Foundations, **2**(1): 51–55. Available from http://www.mendeley.com/research/geology-volcanic-history-eruptive-style-yakedake-volcano-group-central-japan/.

Van Genuchten, M.T. 1980. A closed-form Equation for Predicting the Hydraulic Conductivity of Unsaturated Soils. Soil Science Society of America Journal, **44**(5): 892–898.

Vaniceek, I. 2013. The importance of tensile strength in geotechnical engineering. Acta Geotechnica Slovenica, **10**(1): 5–17. doi:10.1016/0022-2836(71)90334-2.

Varsei, M., Miller, G.A., and Hassanikhah, A. 2016. Novel Approach to Measuring Tensile Strength of Compacted Clayey Soil during Desiccation. International Journal of Geomechanics, **16**(6): D4016011. doi:10.1061/(asce)gm.1943-5622.0000705.

Vesga, L., and Vallejo, L. 2006. Direct and Indirect tensile tests for measuring the equivalent effective stress in a kaolinite clay. In Fourth International Conference on Unsaturated Soils. Carefree, Arizona, United States. pp. 1290–1301.

Wang, J.P., François, B., and Lambert, P. 2020. From Basic Particle Gradation Parameters to Water Retention Curves and Tensile Strength of Unsaturated Granular Soils. International Journal of Geomechanics, **26**(6): 1–10. doi:10.1061/(ASCE)GM.1943-5622.0001677.

Bulolo, S., Leong, E.C. & Kizza, R. (2021). Tensile strength of unsaturated coarse and fine-grained soils. Bull Eng Geol Environ. https://doi.org/10.1007/s10064-020-02073-6

Win, S.S. 2006. Tensile strength of compacted soils subjected to wetting and drying. The University of New South Wales Sydney, Australia.

Wong, C.K., Wan, R.G., and Wong, R.C.K. 2017. Tensile and shear failure behaviour of compacted clay – hybrid failure mode. International Journal of Geotechnical Engineering, **6362**(December): 1–11. Taylor & Francis. doi:10.1080/19386362.2017.1408242.

Yin, P., and Vanapalli, S.K. 2018. Model for predicting tensile strength of unsaturated cohesionless soils. Canadian Geotechnical Journal, **55**(9): 1313–1333. doi:10.1139/cgj-2017-0376.

Young, J.F. 1967. Humidity control in the laboratory using salt solutions-A review. Journal of Applied Chemistry, **17**(9): 241–245. doi:10.1002/jctb.5010170901.

Zeh, R., and Witt, K. 2005. Suction-controlled tensile strength of compacted clays. *In* Proceedings of International Conference on Soil Mechanics and Geotechnical Engineering. pp. 2347–2350.

Table 1. Summary of tensile strength models with consideration of matric suction using the macroscopic approach.

Reference	Tensile strength model's equations
Snyder and Miller (1985)	$\sigma_t = \frac{1}{f(s)}\chi(u_a - u_w)$ where σ_t = tensile stress, f(s) = proportionality factor based on stress concentration of Griffith (1924) fracture criterion and is a function of the degree of saturation, χ = Bishop's chi factor, u_a = pore-air pressure, and u_w = pore-water pressure.
Morris et al. (1992)	$\sigma_t = 0.5\left[c' + (u_a - u_w)\tan\phi^b\right]$ based on Frydman (1967) and Baker (1981) or $\sigma_t = (0.5 \text{ to } 0.7)\left[c' + (u_a - u_w)\tan\phi^b\right]\cot\phi'$ based on Bagge (1985) where c' and ϕ' = effective shear strength parameters, ϕ^b = angle indicating rate of shear strength increase with respect to matric suction.
Lu et al. (2009)	$\sigma_t = \left[2_t \tan\left(\frac{\pi}{4} - \frac{\phi_t}{2}\right)\right]\sigma^s \tan\phi$ where $\sigma^s = \begin{cases} u_w & \text{for } (u_a - u_w) \le 0 \\ S_e(u_a - u_w) & \text{for } (u_a - u_w) \ge 0 \end{cases}$ $S_e = \frac{S - S_r}{1 - S_r}$ $(u_a - u_w) = \frac{1}{\alpha}\left[S_e^{n/(1-n)} - 1\right]^{1/n}$ – van Genuchten (1980) SWCC equation S = degree of saturation, S_e = effective degree of saturation, S_r = residual degree of saturation, α and n = van Genuchten SWCC equation parameters.
(Trabelsi et al. 2012)	$\sigma_t = \frac{2\cos\phi'}{1+\sin\phi'}.\{\sigma_s \tan\phi' + C^*\}$, where $\sigma_s = \frac{A}{\tan\phi'}.\left(\frac{\lvert f(n^*)\rvert + f(n^*)}{2}\right)(u_a - u_w)$ $C^* = B.\left(\frac{\lvert f(n^*)\rvert + f(n^*)}{2}\right)$

	$$f(n^*) = 1 - \left(\frac{n^*}{n^*_0}\right)^p$$ A, B = parameters, n^* = porosity, n^*_0 = reference porosity, and p = material parameter characterizing the shape of the cohesion-porosity function
Tang et al. (2015)	$$\sigma_t = \begin{cases} \left[2\tan\left(\frac{\pi}{4} - \frac{\phi_t}{2}\right)\right] \sigma^s \tan\phi_t & 0 \le S \le S^c \\ \left[2\tan\left(\frac{\pi}{4} - \frac{\phi_t}{2}\right)\right] \sigma^s \tan\phi_t + \sigma_{tr} & S^c \le S \le 100\% \end{cases}$$ where $$\sigma^s = S_e(u_a - u_w)$$ $$(u_a - u_w) = \frac{1}{\alpha}\left[S_e^{n/(1-n)} - 1\right]^{1/n}$$ σ_{tr} = residual tensile strength, and S^c = critical degree of saturation
Varsei et al. (2016)	$$\sigma_t = \frac{2\cos\phi'}{1+\sin\phi'}\left[\sigma_s \tan\phi' + c'\right]$$ where $$\sigma_s = S_e^m (u_a - u_w),$$ $$S_e^m = \frac{S - S_r^m}{1 - S_r^m} = (S)^{\alpha^*}$$ S_r^m = microscopic degree of saturation, and α* = material parameter (always greater than 1).
Yin and Vanapalli (2018)	$$\sigma_t = \left[2_t \tan\left(\frac{\pi}{4} - \frac{\phi_t}{2}\right)\right]\sigma^s \tan\phi$$ where $$\sigma^s = S_e^k (u_a - u_w) + T_s a_{aw}$$ $$k = \begin{cases} \frac{1}{(n-1)} \frac{1}{1 - \left[(0.85 \pm 0.15) S_c\right]^{n/n-1}} & \text{for } C_u \le 6 \\ \frac{1}{(n-1)} \frac{1}{1 - \left[(0.45 \pm 0.15) S_c\right]^{n/n-1}} & \text{for } C_u > 6 \end{cases}$$ $$\frac{S_0}{S_c} = \begin{cases} (0.85 \pm 0.15) & \text{for } C_u \le 6 \\ (0.45 \pm 0.15) & \text{for } C_u > 6 \end{cases}$$

$$a_{aw} = \eta_s \frac{\pi}{e \cdot d_{50}} S_e^{\lambda_s} \left(1 - S_e\right)$$

$$\eta_s = 0.73 C_u$$

$$\lambda_s = \frac{S_r}{1 - S_r}$$

C_u = coefficient of uniformity, S_c = capillary degree of saturation, S_0 = degree of saturation corresponding to the peak tensile strength induced by capillary suction, e = void ratio, d_{50} = diameter at 50% passing.

Wang et al. (2020)

$$\sigma_t = \left[2_t \tan\left(\frac{\pi}{4} - \frac{\phi_t}{2} \right) \right] \sigma^s \tan\phi$$

where

$$\sigma^s = S_e \left(u_a - u_w\right) + T_s a_{aw}$$

$$\left(u_a - u_w\right) = \alpha \left(S_e^{\frac{n}{1-n}} - 1 \right)^{\frac{1}{n}}$$

$$\alpha = \frac{12.07 T_s}{d_{60}}$$

$$n = \frac{1.07}{\log_{10} C_u} + 1;$$

$$a_{aw} = \eta_s \frac{\pi}{e d_{50}} S_e^{\prime s} \left(1 - S_e\right)$$

$$\eta_s = 0.73 Cu$$

$$\lambda_s = 0.3$$

Table 2. Basic properties of the soils used in study

Soil	BT	JF
LL (%)	58	43
PL (%)	31	24
G_s	2.63	2.71
d_{10} (mm)	0.00150	0.00014
d_{30} (mm)	0.002	0.002
d_{50} (mm)	0.005	0.02
d_{50} (mm)	0.009	0.1
Coefficient of Uniformity, C_u	6.0	714.3
Coefficient of Curvature, C_c	0.296	0.286
USCS	MH	CL
Standard Proctor		
Maximum dry density (Mg/m^3)	1.69	1.76
Optimum water content (%)	16.0	16.0
Modified Proctor		
Maximum dry density (Mg/m^3)	1.86	1.94
Optimum water content (%)	13.3	13.5

Table 3. Properties of sample sets A to G in Test Series 2

Soil	Sample set	Average, w (%)	Average, ρ_d (Mg/m^3)	Proctor effort
BT	A	16.0	1.82	Modified
	B	17.5	1.77	Modified
	C	18.0	1.72	Standard
	D	20.5	1.68	Standard
JF	E	17.0	1.84	Modified
	F	18.0	1.75	Standard
	G	20.0	1.70	Standard

Table 4. Shear strength and SWCC equations' parameters for sample sets A – G

Sample set	From CU tests with pore-water pressure measurements		van Genuchten (1980) SWCC equation's parameters	
	ϕ' (°)	c' (kPa)	α (kPa^{-1})	n
A	27.3	8	0.0010	1.670
B	28.2	10	0.0011	1.715
C	28.6	2	0.0013	1.682
D	27.5	5	0.0010	1.675
E	30.0	10	0.0010	1.949
F	29.0	10	0.0013	1.671
G	26.0	10	0.0014	1.737

Table 5. Summary of ϕ_t and RMSE for Lu et al. (2009) tensile strength model

Sample set	Case 1		Case 2	
	$\phi_t = \phi'$ (°)	RMSE	ϕ_t (°) - Fitted	RMSE
A	27.3	682.4	10.0	109.2
B	28.2	382.2	11.0	57.4
C	28.6	580.5	7.0	58.9
D	27.5	835.8	7.0	101.8
E	30.0	476.7	4.0	53.2
F	29.0	918.4	2.0	58.9
G	26.0	506.3	2.0	61.7

Table 6. Summary of parameters and RMSE for Yin and Vanapalli et.al (2018) tensile strength model.

Sample set	Parameters and RMSE	Case 1 $\phi_t = \phi'$	Case 2 ϕ_t - Fitted	Other model parameters
A	η_s	4.38	4.38	e = 0.45 d_{50} = 0.005 mm S_c = 0.91 S_r = 0.0010
	k	3.72	3.72	
	ϕ'	27.3°	10	
	λ_s	0.001	0.001	
	RMSE	159.0	27.2	
B	η_s	4.38	4.38	e = 0.48 d_{50} = 0.005 mm S_c = 0.92 S_r = 0.0140
	k	3.52	3.52	
	ϕ'	28.2°	11	
	λ_s	0.014	0.014	
	RMSE	86.4	40.5	
C	η_s	4.38	4.38	e = 0.515 d_{50} = 0.005 mm S_c = 0.90 S_r = 0.0010
	k	3.61	10.78	
	ϕ'	28.6°	7	
	λ_s	0.001	0.001	
	RMSE	82.6	46.1	
D	η_s	4.38	4.38	e = 0.49 d_{50} = 0.005 mm S_c = 0.91 S_r = 0.0010
	k	3.64	3.64	
	ϕ'	27.5°	7	
	λ_s	0.001	0.001	
	RMSE	82.5	39.4	
E	η_s	73	73	e = 0.44 d_{50} = 0.02 mm S_c = 0.90 S_r = 0.0580
	k	1.49	1.49	
	ϕ'	30°	4	
	λ_s	0.06	0.06	
	RMSE	221.9	69.6	
F	η_s	73	73	e = 0.44 d_{50} = 0.02 mm S_c = 0.90 S_r = 0.0001
	k	1.90	1.90	
	ϕ'	29°	2	
	λ_s	0.0001	0.0001	
	RMSE	215.62	42.57	
G	η_s	73	73	e = 0.505 d50 = 0.02 mm Sc = 0.92 Sr = 0.0065
	k	1.77	1.77	
	ϕ'	26°	2	
	λ_s	0.0066	0.0066	
	RMSE	174.59	46.84	

Table 7. Parameters used in the development of the proposed tensile strength model.

Reference	Soil type	$\phi'(^o)$	c'(kPa)	α (kPa^{-1})	n	S_c	S_r	e	d_{50} (mm)	C_u	Cc	P_{200} (%)
Test data Set A	Fine grained (MH)	27.3	8	0.0009	1.710	0.91	0.001	0.45	0.005	6.00	0.296	72
Test data Set B	Fine grained (MH)	28.2	10	0.0010	1.725	0.92	0.014	0.48	0.005	6.00	0.296	72
Test data Set C	Fine grained (MH)	28.6	2	0.0013	1.682	0.90	0.0	0.52	0.005	6.00	0.296	72
Test data Set D	Fine grained (MH)	27.5	5	0.0012	1.675	0.91	0.001	0.49	0.005	6.00	0.296	72
Test data Set E	Fine grained (CL)	30.0	10	0.0012	1.949	0.90	0.058	0.44	0.020	714.29	0.286	58
Test data Set F	Fine grained (CL)	29.0	10	0.0014	1.671	0.90	0.0	0.44	0.020	714.29	0.286	58
Test data Set G	Fine grained (CL)	26.0	10	0.0014	1.757	0.92	0.007	0.51	0.020	714.29	0.286	58
Goulding (2006)	F-75 Dense sand	27.3	0	0.3011	4.527	0.95	0.015	0.65	0.210	1.733	0.926	39
	F-75 Loose sand	27.3	0	0.2741	4.527	0.95	0.015	0.75	0.210	1.73	0.926	39
	F-55 Dense sand	28.0	0	0.3960	4.261	0.95	0.001	0.65	0.250	1.5	0.996	24
	F-55 Loose sand	28.0	0	0.3960	4.361	0.93	0.001	0.75	0.250	1.5	0.996	24
	F-40 Dense sand	30.0	0	0.3050	5.002	0.94	0.001	0.65	0.330	1.52	0.825	15
	F-40 Loose sand	30.0	0	0.3050	5.002	0.92	0.001	0.75	0.330	1.52	0.825	15
Lu et al. (2007)	Silty Sand	48.0	0	0.2500	3.750	0.92	0.020	0.82	0.110	1.83	0.742	96
	Fine Sand	48.0	0	0.1811	3.409	0.94	0.048	0.82	0.170	1.31	0.652	83
Lu et al. (2009)	Medium Sand	48.0	0	0.7091	3.760	0.93	0.001	0.67	0.450	1.52	0.747	0
	Esperance Sand	48.0	0	0.8295	4.109	0.92	0.093	0.82	0.230	2.00	0.781	40
Narvaez et al. (2015)	Tailing A (ML)	35.2	0	0.0056	2.145	0.91	0.0	0.84	0.012	9.5	1.684	98
	Tailing B (ML)	35.0	0	0.0125	2.468	0.92	0.010	0.79	0.030	14	2.294	99
	Tailing C (ML)	35.0	0	0.0018	2.100	0.92	0.001	0.81	0.021	20.00	0.800	100

Table 8. Correlation matrix for coarse-grained soils

Parameter	α	n	e	d_{50}	C_u	C_c	P_{200} (%)	$\alpha.C_u$	$\alpha.C_c$	$n.C_u$	$n.C_c$	$e.P_{200}$	e.n
A	-0.0922	0.0677	-0.5721	0.0231	-0.1077	0.9247	-0.4212	-0.1441	0.1568	0.0441	0.2954	-0.4791	-0.1210
k_1	0.0737	-0.5950	0.4269	-0.2261	-0.2739	-0.6682	0.4884	0.0740	-0.0531	-0.6723	-0.7230	0.5096	0.0741
k_{1_2}	0.1316	-0.7070	0.5667	-0.3692	-0.1289	-0.5765	0.6072	0.1368	0.0226	-0.7391	-0.7890	0.6351	0.1451

Table 9. Correlation matrix for fine-grained soils

Parameter	α	n	e	d_{50}	C_u	C_c	P_{200} (%)	$\alpha.C_u$	$\alpha.C_c$	$n.C_u$	$n.C_c$	$e.P_{200}$	e.n
A	0.9416	0.9568	0.8165	0.4889	-0.3912	0.9859	0.7942	-0.3126	0.9246	-0.3820	0.9815	0.8237	0.9107
k_1	-0.7812	-0.8649	-0.8982	-0.5768	0.3166	-0.8554	-0.8163	0.1937	-0.7471	0.3197	-0.8422	-0.8814	-0.9189
k_{1_2}	-0.7950	-0.9198	-0.8685	-0.5613	0.3507	-0.8763	-0.8321	0.2750	-0.7733	0.3406	-0.8664	-0.8732	-0.9204

Table 10. Parameters of validation data used in the proposed tensile strength model.

Reference	Win (2006)	Kim and Sture (2008)	Jindal et al. (2016)	Zeh and Witt (2005)	Wong et al. (2017)	Murray and Tarantino (2019)
Soil type	Clayey sand	Medium sand	Silica sand	Clay	Clay	Vitreous Clay
Tensile test	Direct	Direct	Uniaxial	Direct	Uniaxial	Uniaxial
c'(kPa)	0.0	0.0	0	16.8	27.9	0
$\phi'(^{o})$	25.0	32.0	48.0	25.0	32.3	27.8
n	1.655	4.145	4.492	1.578	2.253	2.115
α (kPa^{-1})	0.0005	0.4051	0.402	0.0007	0.0024	0.0006
S_r	0.0000	0.0000	0.0000	0.0000	0.0000	0.0000
e	0.53	0.80	0.61	0.80	0.72	0.53
P_{200} (%)	47	0	0	98	100	55
C_u	50.00	1.79	1.84	23.33	5.00	64.29
C_c	0.81	0.83	0.89	0.80	0.288	1.14

Table 11. Comparison of RMSE of the validation data for proposed, Lu et al. (2009) and Yin and Vanapalli (2018) tensile strength models.

Reference	Proposed	Lu at al. (2009)	Yin and Vanapalli (2018)
Win (2006)	10.16	862.90	673.84
Kim and Sture (2008)	0.24	0.46	0.42
Jindal et al. (2016)	0.11	1.40	0.95
Zeh and Witt (2005)	119.36	1394.45	509.37
Wong et al. (2017)	6.65	113.68	217.56
Murray and Tarantino (2019)	89.03	243.43	235.09

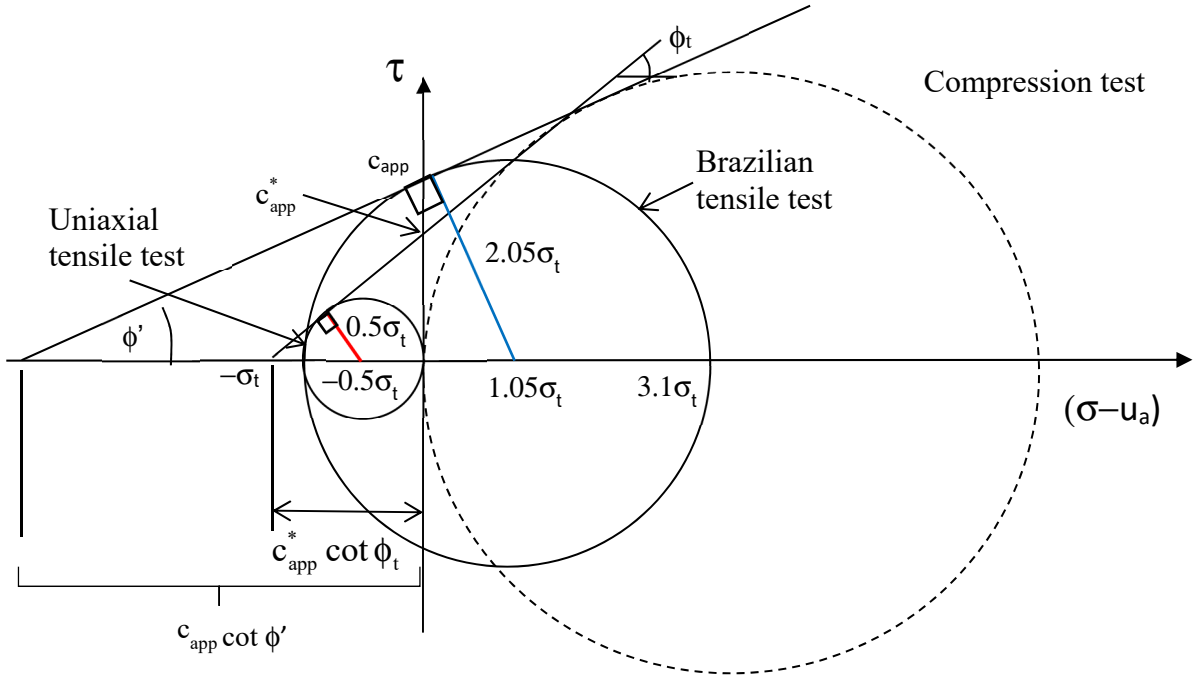

Figure 1. Representations of Uniaxial and Brazilian tensile strength tests using Mohr-Coulomb failure criterion.

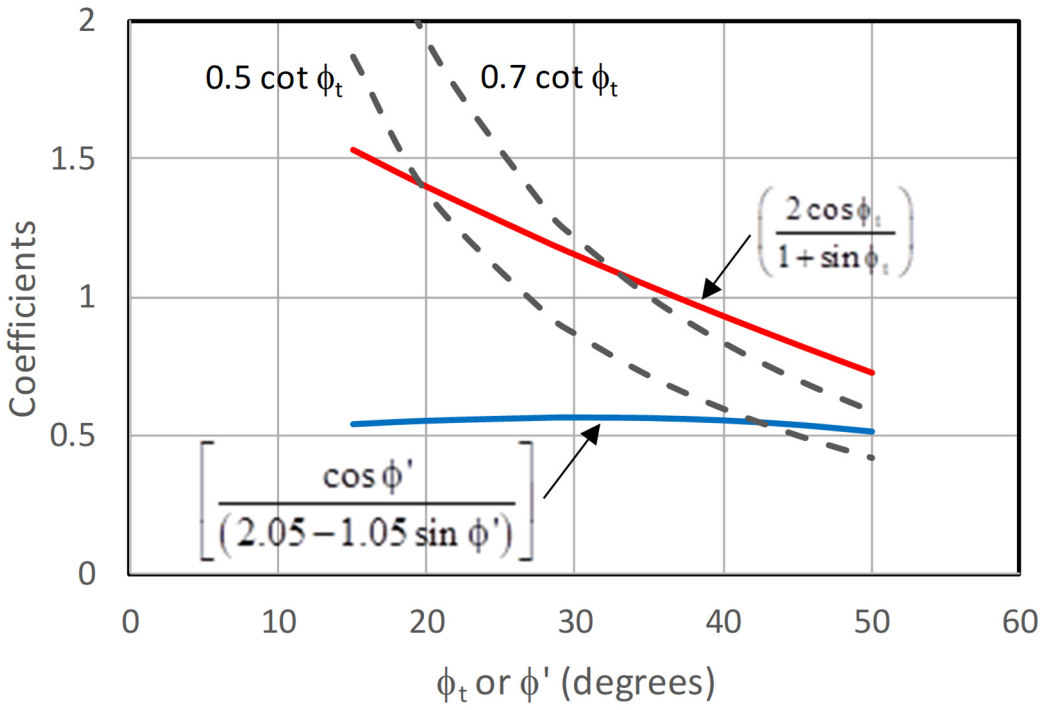

Figure 2. Comparison of coefficients in Equations 1 and 2 with Morris et al. (1992) model.

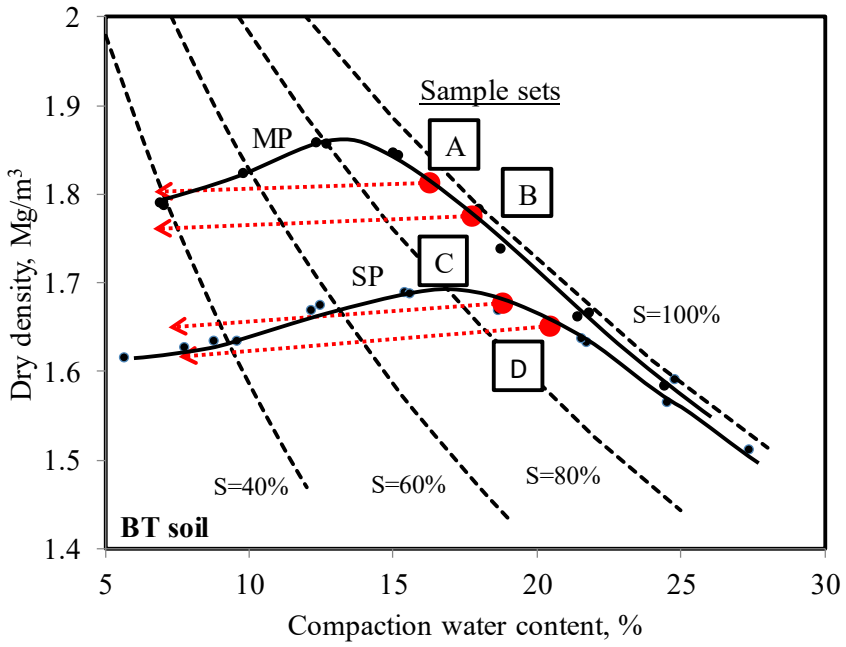

(a) BT soil

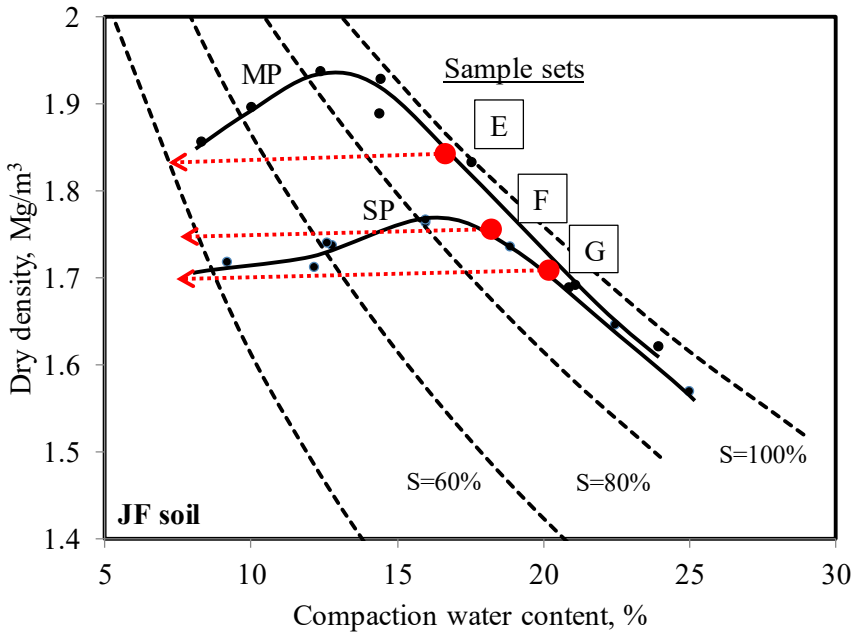

(b) JF soil

Figure 3. Compaction curves and sample sets

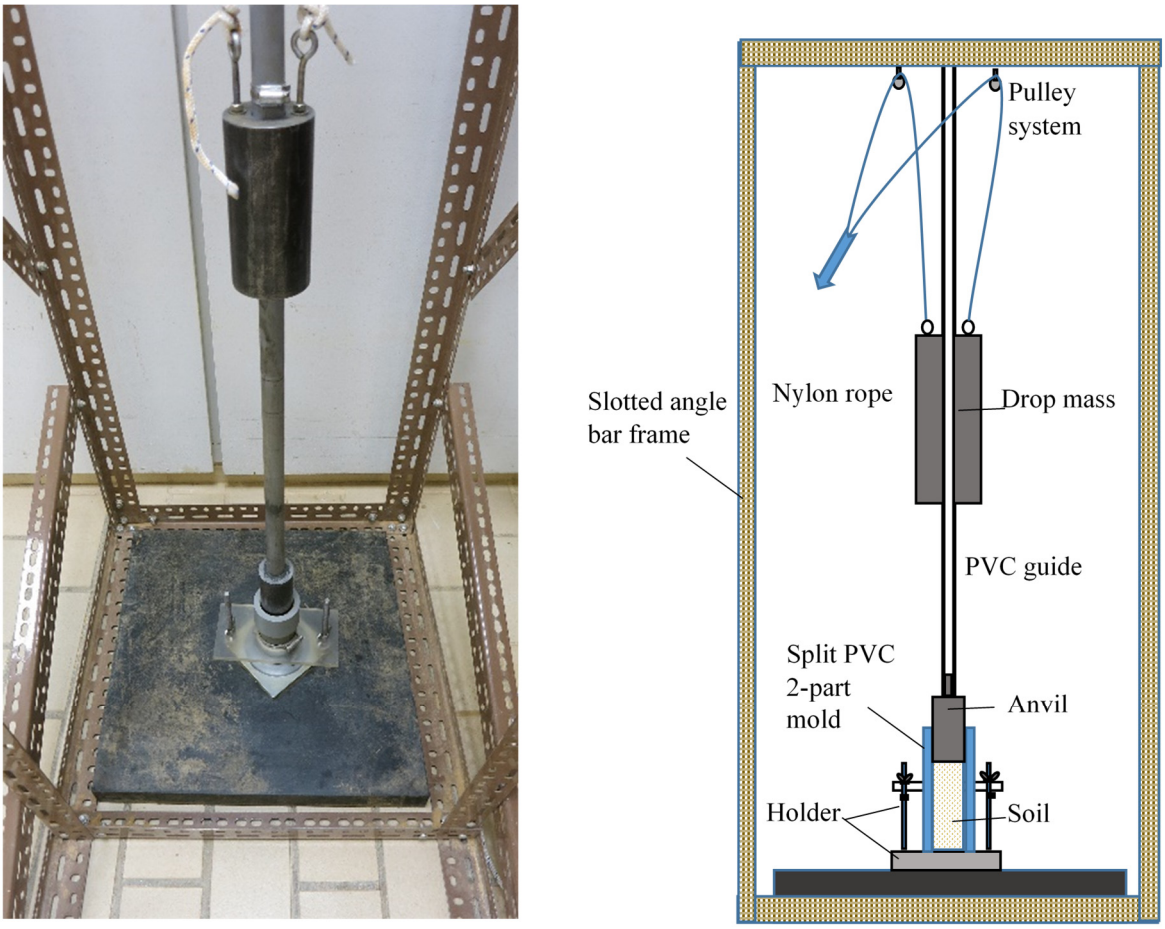

(a) Photo

(b) Schematic drawing

Figure 4. Compaction set-up to prepare soil specimens in PVC mold

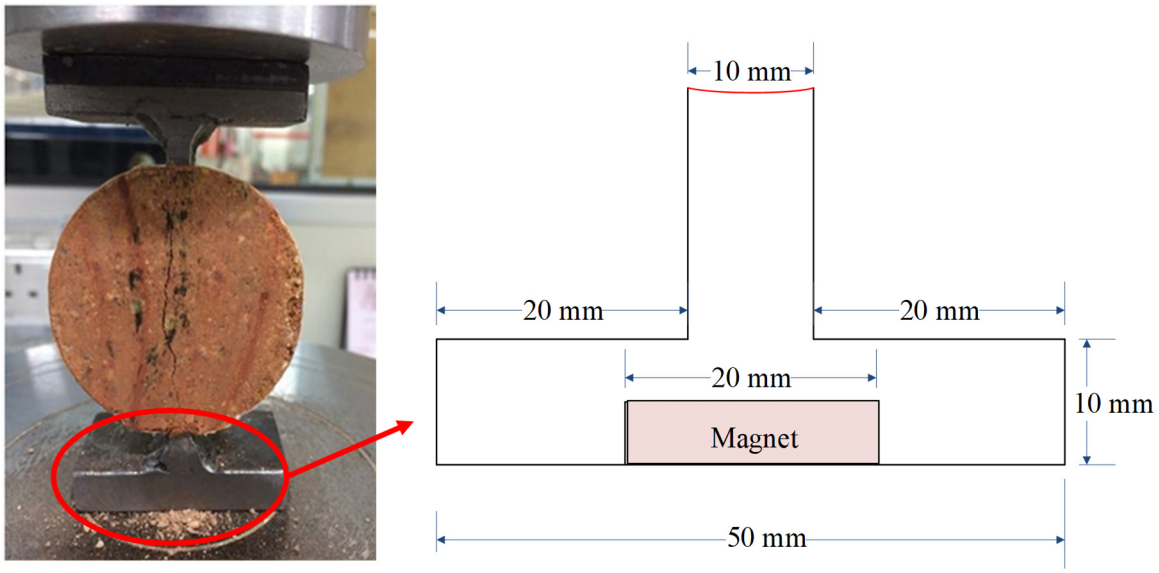

(a) Test set-up (b) Curved bearing block

Figure 5. Brazilian test set-up and curved bearing block

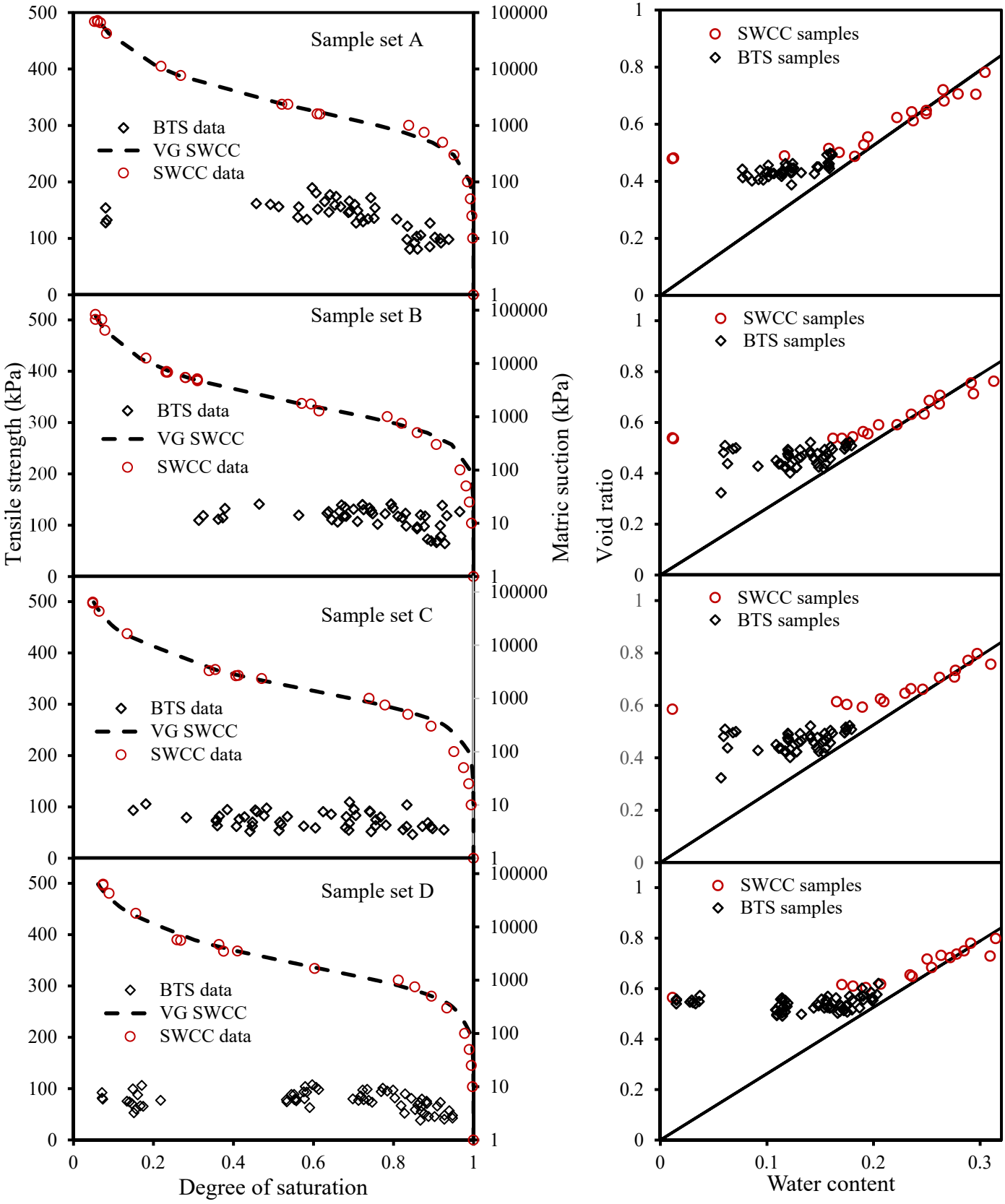

Figure 6a. Summary of test results for sample sets A to D

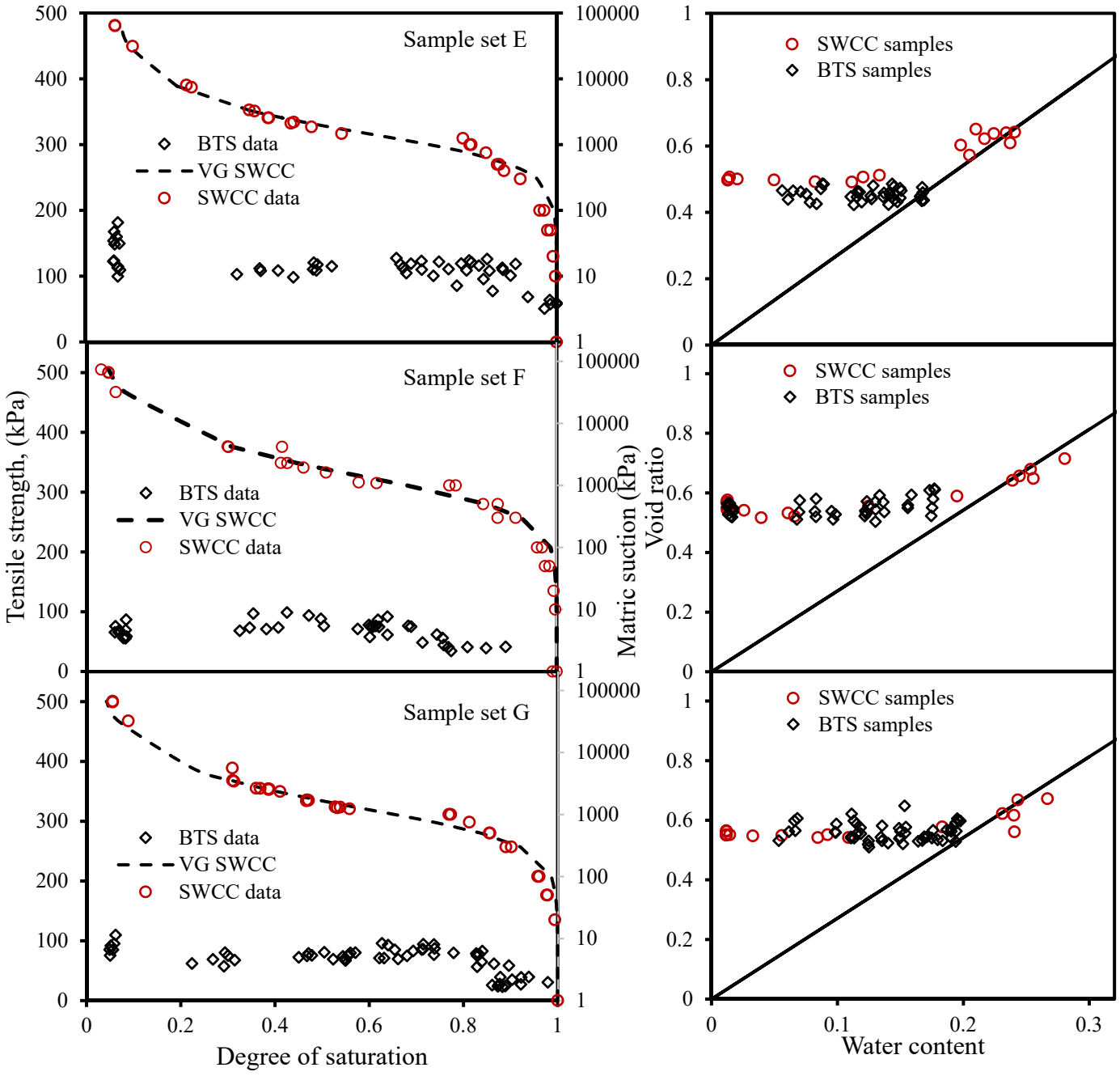

Figure 6b. Summary of test results for sample sets E to G

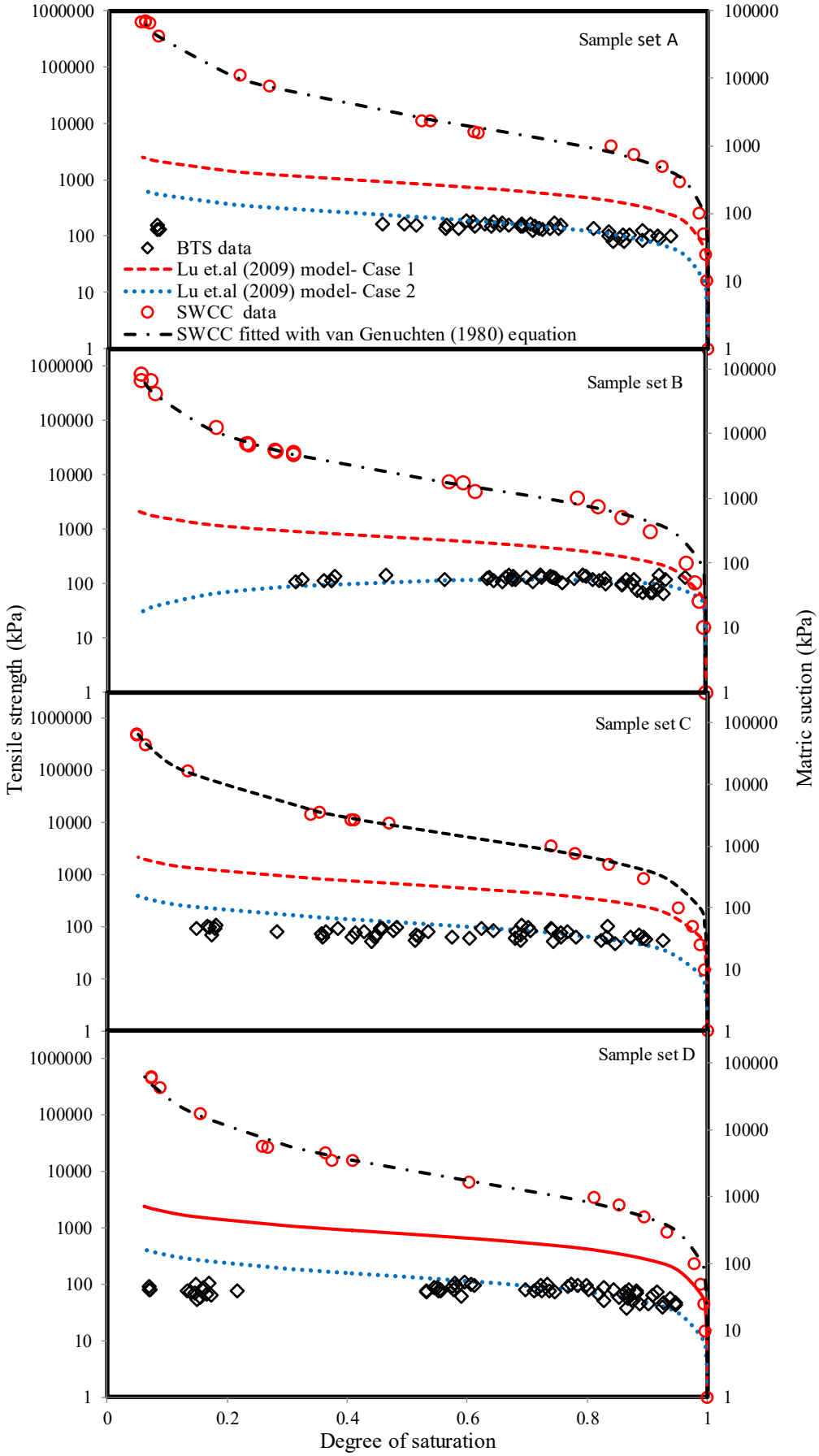

Figure 7a. Evaluation of Lu et al. (2009) tensile strength model (Sample sets A-D)

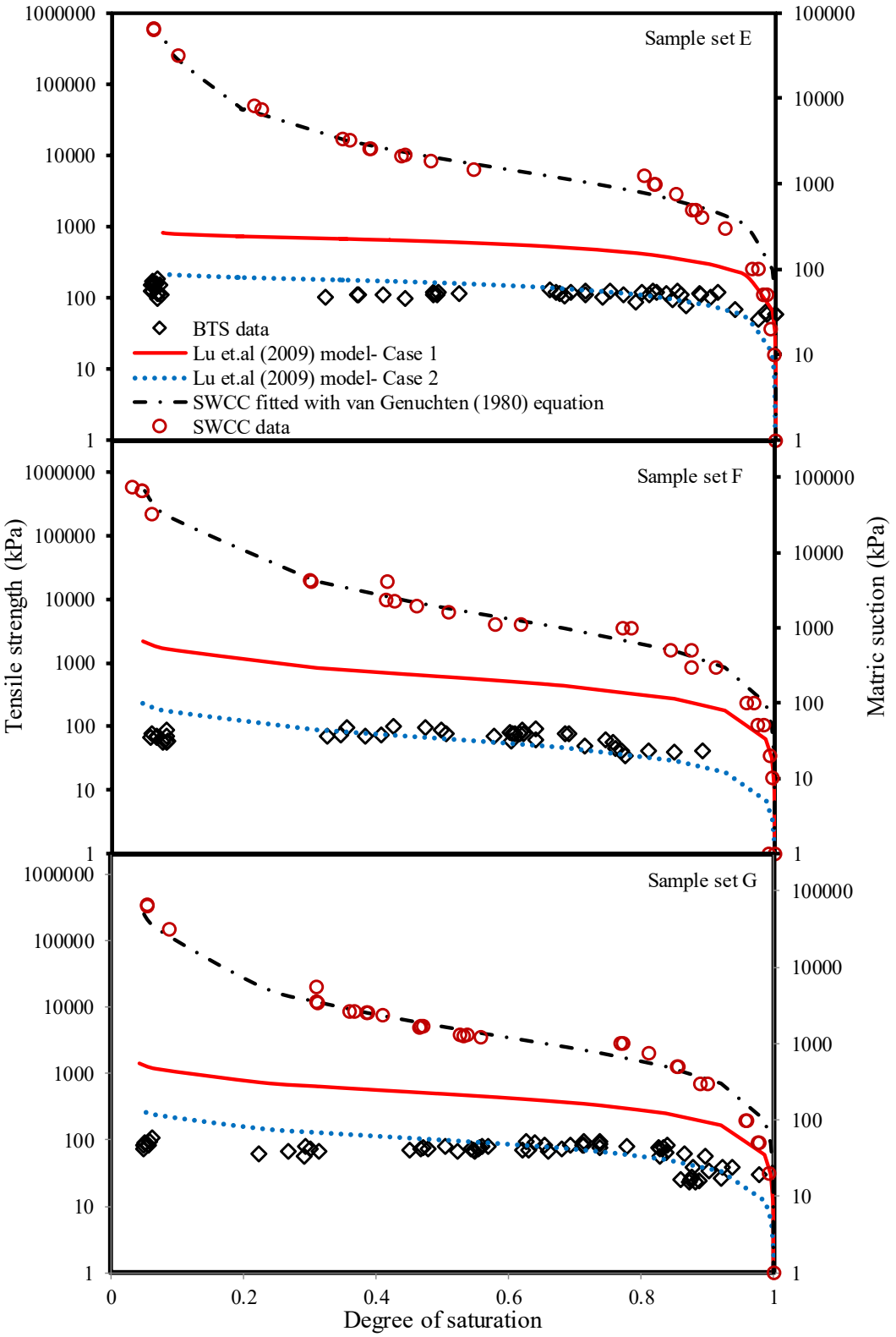

Figure 7b. Evaluation of Lu et al. (2009) tensile strength model (Sample sets E - G)

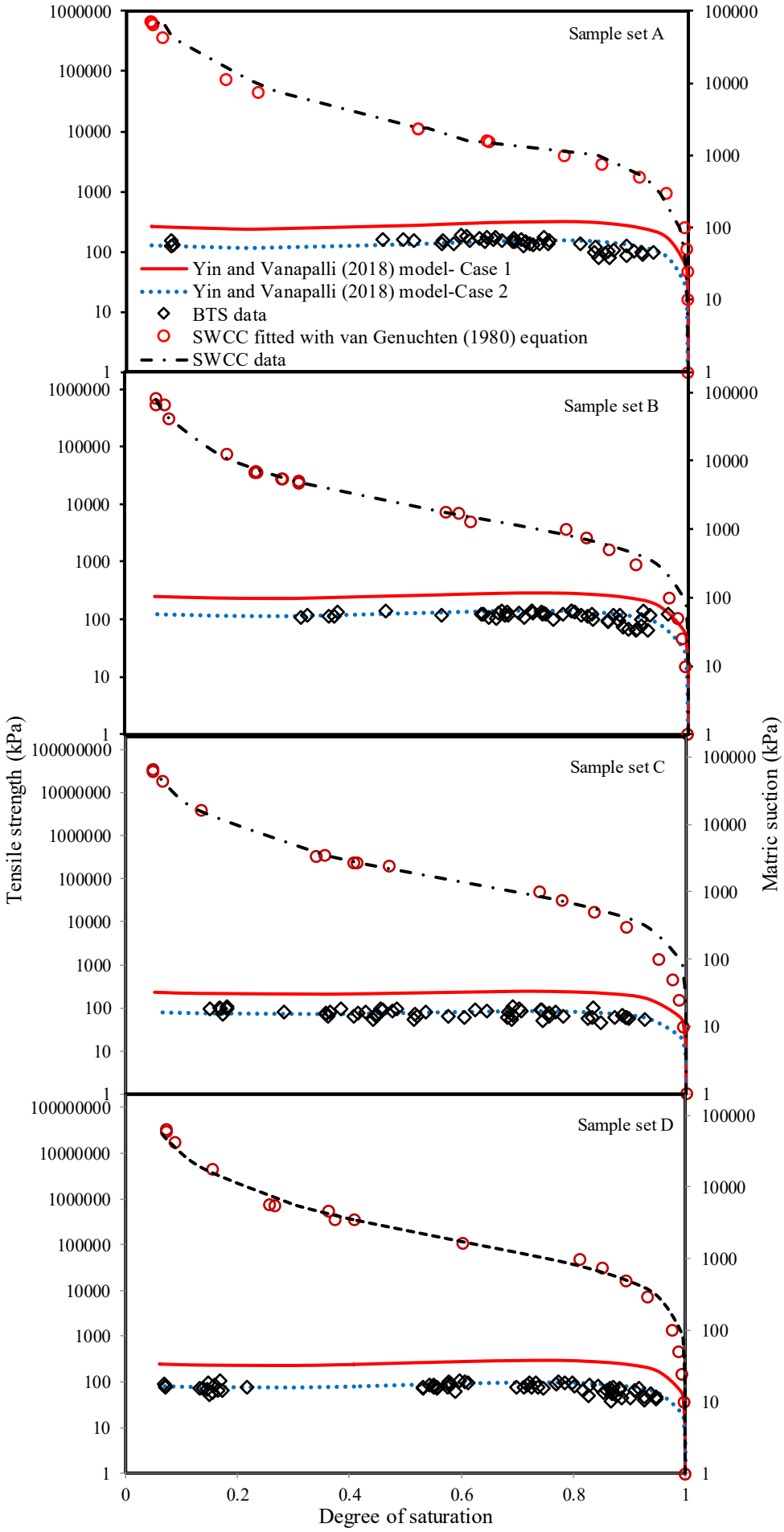

Figure 8a. Evaluation of Yin and Vanapalli (2018) tensile strength model (Sample sets A – D)

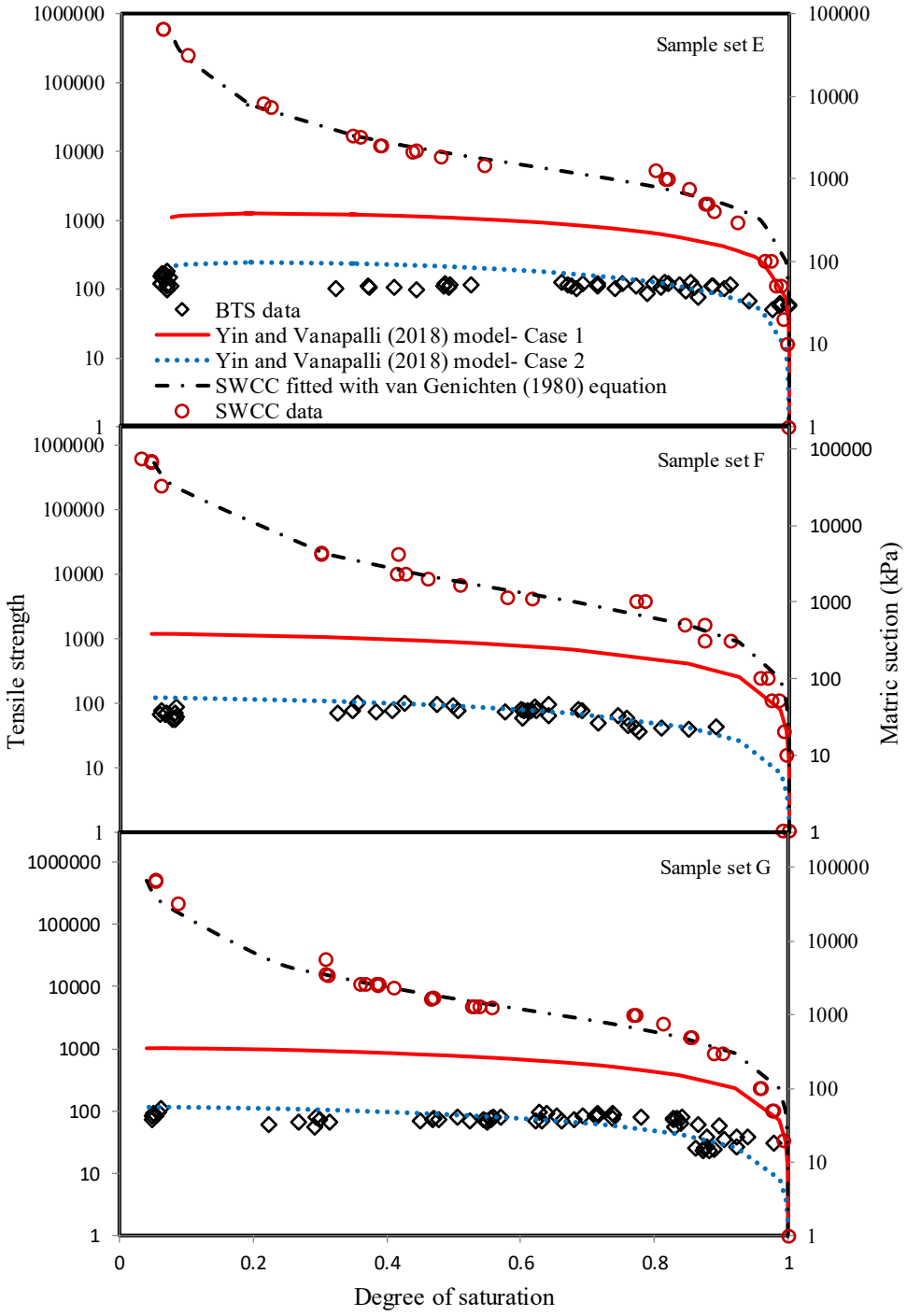

Figure 8b. Evaluation of Yin and Vanapalli (2018) tensile strength model (Sample sets E – G)

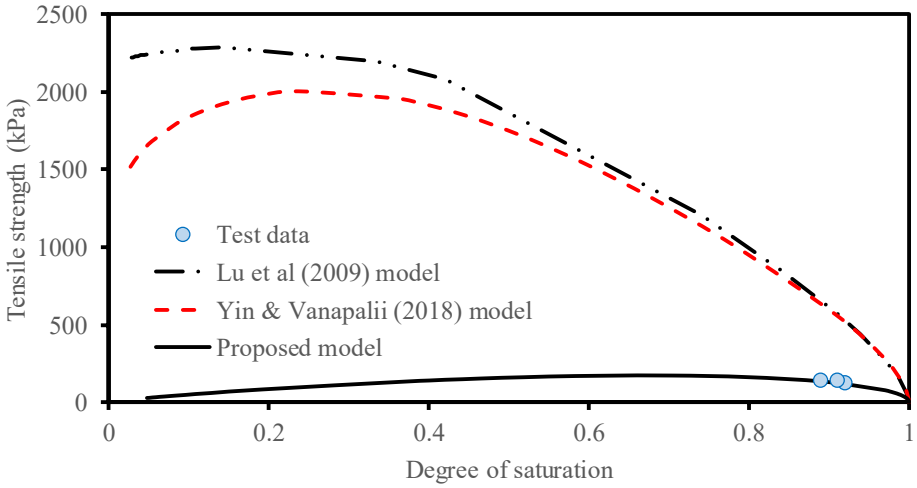

(a) Data from Win (2006)

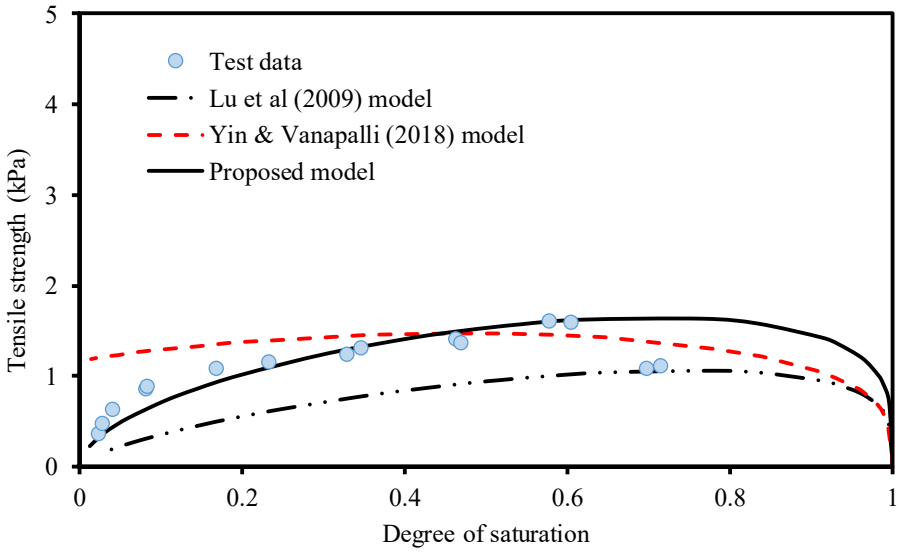

(b) Data from Kim and Sture (2008)

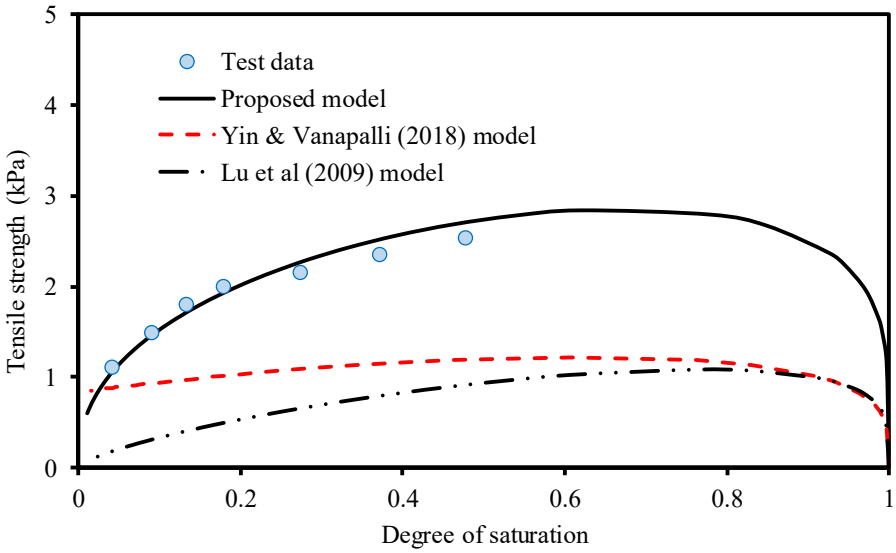

(c) Data from Jindal et al. (2016)

Figure 9. Validation of proposed tensile strength model for coarse-grained soils

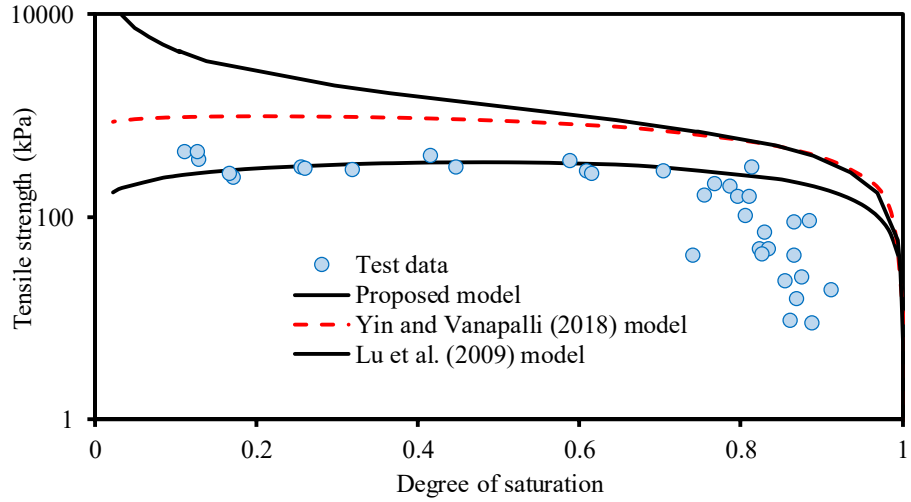

(a) Data from Zeh and Witt (2005)

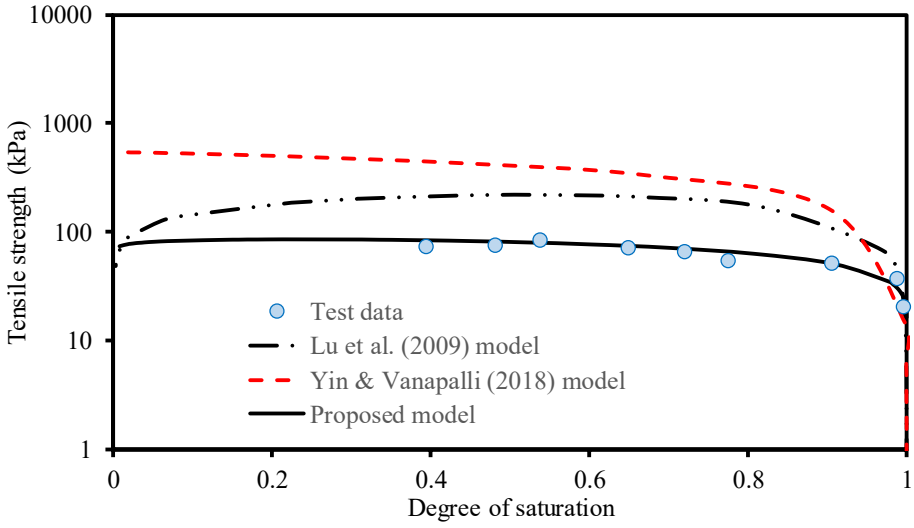

(b) Data from Wong et al. (2017)

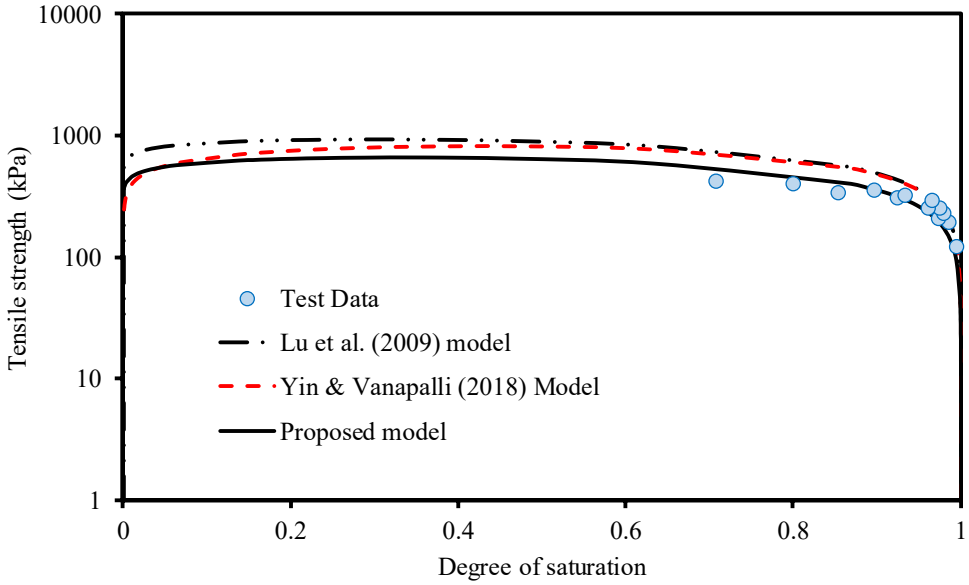

(c) Data from Murray and Tarantino (2019)

Figure 10. Validation of proposed tensile strength model for fine-grained soils